Science Advances
AAAS

Supplementary Materials for

Discovery of DRP-104, a tumor-targeted metabolic inhibitor prodrug

Rana Rais *et al.*

Corresponding author: Barbara S. Slusher, bslusher@jhmi.edu; Rana Rais, rrais2@jhmi.edu

Sci. Adv. **8**, eabq5925 (2022)
DOI: 10.1126/sciadv.abq5925

The PDF file includes:

Other Supplementary Material for this manuscript includes the following:

Data tables for Figs. 2 to 8
Data tables for figs. S2, S4 to S8, and S10 to S13
Data table for top polar metabolites (for metabolomics Fig. 6)
Raw data for Fig. 6B

RESULTS

Synthesis of DON peptide prodrugs P1-8

We synthesized a series of dipeptide prodrugs with various ester linkages on R_1 (**Figure S1**) and subsequently modified the R_2 groups to obtain prodrugs with optimal properties. The goal was to enhance the stability of the ester linkage at R_1 while maintaining tumor partitioning. On the R_1 moiety we introduced isopropyl (**P1-3**), 1,3-difluoropropan-2-yl (**P4**), d_3-methyl (**P5**), and 2-(2-methoxyethoxy)ethan-1-yl (**P6-7**) groups in attempt to enhance stability by imparting steric hindrance. In addition, an amide analog (**P8**) was synthesized as amides are less prone to hydrolysis than esters. Modifications on the R_2 moiety included quinuclidine-4-yl (**P1**), 1-(4-methylpiperazine-1-yl)methyl (**P2**), acetyl (**P3-6,8**) and 2-(dimethylamino)methyl (**P7**).

Metabolic stability and tumor partitioning analysis of P1-8

Prodrugs **P1-8** were screened for metabolic stability in gastrointestinal homogenates and DON release in a tumor cell partitioning assay following methods reported previously (*74*, *80*). The metabolic stability of the prodrugs in GI tissue homogenates is presented in **Figure S2**. Various R_1 and R_2 promoiety changes in **P1**-**P7** did not improve GI tissue stability. Modification of the R_1 promoiety from ester to amino (**P8**), however, resulted in enhanced stability with >50% remaining at 1h. Interestingly, although **P1-7** were unstable in GI tissues, the total DON release was less than 10%. Metabolite identification (Met-ID) studies revealed partial hydrolysis of **P1-7** at the R_1 moiety resulting in the formation of an intermediate with free carboxylate (*data not shown*). Prodrugs were next tested our *in vitro* tumor partitioning assay for analysis of DON release in tumor cells. Briefly, **P1-8** were incubated (20 µM) for 1h in a P493B lymphoma cell suspended in 1 mL human plasma and DON release was measured in plasma and tumor cells as described(*80*). All prodrugs showed minimal release of DON in human plasma as well as

tumors, except for **P3 (DRP-104)** (with isopropyl as R_1 moiety and acetyl as R_2 moiety) which delivered the highest DON tumor levels. Given these data, **DRP-104** was selected for further characterization. (**Fig. S2**).

METHODS

Synthesis and characterization of prodrugs P1-P8

All chemicals were purchased from Sigma-Aldrich or TCI and were used without further purification. The commercially available HPLC grade acetonitrile, catalysts and reagent grade materials were used as received. The ^{1}H NMR spectra were measured at 400.1 or 600.1 MHz in $CDCl_3$ or DMSO-d_6. For standardization of ^{1}H NMR spectra the internal signal of TMS (δ 0.0, $CDCl_3$) or residual signals of solvents (δ 7.26 for $CDCl_3$ and δ 2.50 for DMSO-d_6) were used. The chemical shifts are given in δ-scale, and the coupling constants J are given in Hz. The ESI mass spectra were recorded using ZQ micromass mass spectrometer (Waters) equipped with an ESCi multimode ion source and controlled by MassLynx software. The purity of all compounds subjected to biological testing was established using HPLC (Jasco Inc.) equipped with a Reprosil 100 C18, 5 μm, 250 × 4 mm column. The analysis was performed using a gradient of 2% CH_3CN / 98% H_2O with 0.1% TFA → 100% CH_3CN, with UV detection, λ = 210 nm. Purity of all compounds subjected to biological testing was over 95%.

L-Pyroglutamic acid was refluxed with respective alcohol containing the R_1 (**a-d**) in the presence of p-toluenesulfonic acid to give the respective ester (**2a-d**). The amide nitrogen then was masked using Fmoc-Cl to give Fmoc-protected ester of L-pyroglutamic acid (**3a-d**). These esters (**3a-d**) were transformed to Fmoc-protected (*S*)-2-amino-6-diazo-5-oxohexanoate esters (**4a-d**) by cleavage of the C-N amide bond triggered by alkylation using trimethylsilyl diazomethane. The 2-(2-methoxyethoxy)ethyl ester (**4e**) was synthesized upon removal of R_1

(allyl) group of **4d** followed by conjugation with 2-(2-methoxyethoxy)ethan-1-ol. All the resulting Fmoc-protected esters (**4a-e**) were deprotected to free amine (**5a-e**). Compounds **5a-e** were then coupled with Fmoc-protected L-tryptophan to yield the conjugates **6a-e** followed by the deprotection of the Fmoc group to yield primary amines **7a-e**. These compounds were then coupled with respective acids / acetic anhydride / AcOSu / dimethylglycineOSu to yield the prodrugs **P1- P7**. **P8** was synthesized from **P3** by amidation using 7M NH_3 in methanol. All intermediates were isolated, purified by column chromatography and characterized using ^{1}H NMR spectroscopy and high-resolution MS. NMR spectra and high-resolution MS characterization data of **P1-P8** are given below.

P1	**^{1}H NMR** (DMSO-d_6): 1.18 (d, *J* = 2.7 Hz, 3H), 1.20 (d, *J* = 2.7 Hz, 3H), 1.41 – 1.51 (m, 6H), 1.77 – 1.90 (m, 1H), 1.92 – 2.06 (m, 1H), 2.36 – 2.44 (m, 2H), 2.67 – 2.75 (m, 6H), 3.01 (dd, *J* = 14.7, 9.5 Hz, 1H), 3.13 (dd, *J* = 14.6, 4.3 Hz, 1H), 4.14 – 4.27 (m, 1H), 4.55 (td, *J* = 8.9, 4.2 Hz, 1H), 4.91 (hept, *J* = 6.2 Hz, 1H), 6.03 (bs, 1H), 6.97 (ddd, *J* = 8.0, 7.0, 1.1 Hz, 1H), 7.05 (ddd, *J* = 8.1, 6.9, 1.2 Hz, 1H), 7.13 (d, *J* = 2.4 Hz, 1H), 7.17 (d, *J* = 8.1 Hz, 1H), 7.31 (dt, *J* = 8.1, 0.9 Hz, 1H), 7.60 (d, *J* = 7.9 Hz, 1H), 8.29 (d, *J* = 7.5 Hz, 1H), 10.77 (bs, 1H). **HR ESI MS**: calcd for $C_{28}H_{36}O_5N_6Na$ 559.26394; found 559.26353.
P2	**^{1}H NMR** ($CDCl_3$): 1.22 (d, *J* = 6.2 Hz, 3H), 1.24 (d, *J* = 6.3 Hz, 3H), 1.88 – 2.01 (m, 1H), 2.10 – 2.25 (m, 6H), 2.25 – 2.35 (m, 3H), 2.34 – 2.51 (m, 2H), 2.81 – 3.05 (m, 5H), 3.19 – 3.38 (m, 2H), 4.43 (td, *J* = 7.7, 4.6 Hz, 1H), 4.73 (q, *J* = 6.9 Hz, 1H), 4.98 (hept, *J* = 6.2 Hz, 1H), 5.22 (bs, 1H), 6.68 (d, *J* = 7.4 Hz, 1H), 7.08 – 7.15 (m, 2H), 7.19 (ddd, *J* = 8.2, 7.1, 1.3 Hz, 1H), 7.36 (dt, *J* = 8.1, 1.0 Hz, 1H), 7.61 – 7.70 (m, 2H), 8.23 (bs, 1H). **HR ESI MS**: calcd for $C_{27}H_{38}O_5N_7$ 540.29289; found 540.29246.

P3	**^{1}H NMR** (401MHz, DMSO-d_6): δH 1.18 (d, J = 6.3 Hz, 3H), 1.19 (d, J = 6.3 Hz, 3H), 1.77 (s, 3H), 1.78 – 1.89 (m, 1H), 1.95 – 2.05 (m, 1H), 2.30 – 2.46 (m, 2H), 2.89 (dd, J = 14.8, 9.7 Hz, 1H), 3.11 (dd, J = 14.8, 4.3 Hz, 1H), 4.20 (ddd, J = 9.3, 7.4, 5.2 Hz, 1H), 4.58 (ddd, J = 9.7, 8.1, 4.3 Hz, 1H), 4.90 (hept, J = 6.3 Hz, 1H), 6.03 (bs, 1H), 6.99 (ddd, J = 8.0, 7.0, 1.1 Hz, 1H), 7.06 (ddd, J = 8.1, 6.9, 1.2 Hz, 1H), 7.16 (d, J = 2.4 Hz, 1H), 7.33 (d, J = 8.1 Hz, 1H), 7.63 (d, J = 7.9 Hz, 1H), 8.04 (d, J = 8.1 Hz, 1H), 8.43 (d, J = 7.5 Hz, 1H), 10.81 (d, J = 2.5 Hz, 1H). **HR ESI MS**: calcd for $C_{22}H_{27}N_5O_5Na$ 464.19044; found 464.19050.
P4	**^{1}H NMR** ($CDCl_3$): 1.82 – 1.94 (m, 1H), 1.91 (s, 3H), 2.00 – 2.11 (m, 1H), 2.12 – 2.26 (m, 2H), 3.15 (d, *J* = 6.6 Hz, 2H), 4.34 (td, *J* = 7.7, 4.7 Hz, 1H), 4.45 (t, *J* = 4.1 Hz, 2H), 4.57 (t, *J* = 4.1 Hz, 2H), 4.61 – 4.70 (m, 1H), 5.15 (tt, *J* = 19.5, 4.6 Hz, 1H), 5.22 (bs, 1H), 6.78 (d, *J* = 7.9 Hz, 1H), 7.00 – 7.08 (m, 2H), 7.12 (t, *J* = 7.5 Hz, 1H), 7.31 (d, *J* = 8.0 Hz, 1H), 7.47 (d, *J* = 7.3 Hz, 1H), 7.56 (d, *J* = 7.8 Hz, 1H), 9.06 (s, 1H). **HR ESI MS**: calcd for $C_{22}H_{25}O_5N_5F_2Na$ 500.17160; found 500.17202.
P5	**^{1}H NMR** ($CDCl_3$): 1.82 – 1.95 (m, 1H), 1.98 (s, 3H), 2.04 – 2.13 (m, 1H), 2.14 – 2.34 (m, 2H), 3.17 (dd, *J* = 14.6, 7.3 Hz, 1H), 3.32 (dd, *J* = 14.6, 5.4 Hz, 1H), 4.40 (td, *J* = 7.7, 4.6 Hz, 1H), 4.76 (td, *J* = 7.5, 5.3 Hz, 1H), 5.15 (bs, 1H), 6.27 (d, *J* = 7.7 Hz, 1H), 6.72 (d, *J* = 7.2 Hz, 1H), 7.07 – 7.14 (m, 2H), 7.18 (ddd, *J* = 8.1, 7.0, 1.2 Hz, 1H), 7.35 (d, *J* = 7.9 Hz, 1H), 7.65 (d, *J* = 7.8 Hz, 1H), 8.38 (bs, 1H). **HR ESI MS**: calcd for $C_{20}H_{20}D_3O_5N_5Na$ 439.17740; found 439.17797.
P6	**^{1}H NMR** ($CDCl_3$): 1.88 (dt, *J* = 14.1, 7.0 Hz, 1H), 1.97 (s, 3H), 2.06 (p, *J* = 5.6, 4.2 Hz, 1H), 2.12 – 2.30 (m, 2H), 3.22 (ddd, *J* = 56.3, 14.5, 6.4 Hz, 2H), 3.36 (s, 3H), 3.50 – 3.71 (m, 6H), 4.21 (dtd, *J* = 21.1, 12.2, 10.8, 5.8 Hz, 2H), 4.41 (q, *J* = 7.2, 6.7 Hz, 1H), 4.75 (q, *J* = 6.9 Hz, 1H), 5.20 (bs, 1H), 6.44 (d, *J* = 7.6 Hz, 1H), 6.73 (d, *J* =

	7.4 Hz, 1H), 7.03 – 7.18 (m, 3H), 7.33 (d, *J* = 8.1 Hz, 1H), 7.65 (d, *J* = 7.9 Hz, 1H), 8.83 (s, 1H). **HR ESI MS**: calcd for $C_{24}H_{31}O_7N_5Na$ 524.21157; found 524.21106.
P7	**^{1}H NMR** (DMSO-d_6): 1.81 – 1.90 (m, 1H), 1.94 – 2.08 (m, 7H), 2.35 – 2.44 (m, 2H), 2.75 (dt, *J* = 31.2, 15.8 Hz, 2H), 3.14 – 3.19 (m, 2H), 3.20 (s, 3H), 3.40 (dd, *J* = 5.8, 3.7 Hz, 2H), 3.52 (dd, *J* = 5.9, 3.6 Hz, 2H), 3.60 (t, *J* = 4.9 Hz, 2H), 4.04 – 4.17 (m, 1H), 4.17 – 4.25 (m, 1H), 4.25 – 4.31 (m, 1H), 4.61 – 4.69 (m, 1H), 6.02 (bs, 1H), 6.97 (t, *J* = 7.4 Hz, 1H), 7.05 (t, *J* = 7.5 Hz, 1H), 7.12 – 7.16 (m, 1H), 7.31 (d, *J* = 8.1 Hz, 1H), 7.56 – 7.67 (m, 2H), 8.52 (d, J = 7.5 Hz, 1H), 10.81 (s, 1H). **HR ESI MS**: calcd for $C_{26}H_{37}O_7N_6$ 545.27182; found 545.27157.
P8	**^{1}H NMR** (DMSO-d_6): 1.68 – 1.78 (m, 1H), 1.79 (s, 3H), 1.87 – 2.00 (m, 1H), 2.20 – 2.32 (m, 2H), 2.91 (dd, *J* = 14.7, 9.1 Hz, 1H), 3.12 (dd, *J* = 14.7, 4.7 Hz, 1H), 4.15 (td, *J* = 8.6, 5.1 Hz, 1H), 4.49 (ddd, *J* = 9.1, 7.5, 4.7 Hz, 1H), 5.99 (bs, 1H), 6.97 (t, *J* = 7.4 Hz, 1H), 7.02 – 7.10 (m, 2H), 7.12 – 7.22 (m, 2H), 7.32 (d, *J* = 8.0 Hz, 1H), 7.60 (d, *J* = 7.9 Hz, 1H), 7.99 (d, *J* = 8.0 Hz, 1H), 8.05 (d, *J* = 7.6 Hz, 1H), 10.80 (bs, 1H). **HR ESI MS**: calcd for $C_{19}H_{22}O_4NaN_6$ 421.15947; found 421.15918.

Metabolic stability and tumor partitioning analysis of P1-8

The metabolic stability analysis of prodrugs **P1-8** were performed in mouse GI (jejunum) tissue homogenates as previously described(*74, 80*). Briefly, tissue homogenates were prepared in 0.1 M potassium phosphate buffer (10-fold dilution) using a probe sonicator. 1 mL aliquots of the tissue homogenates were spiked with a final assay concentration of 10 μM of each prodrug followed by incubation in an orbital shaker at 37 °C for 1 h (in triplicate). Samples from each incubation at t = 0 and 1h were quenched with five volumes of methanol containing the internal standards (IS; losartan: 0.5 μM; glutamate-d_5: 10 μM). Samples were vortex-mixed for 30 s and centrifuged at 10,000 × *g* for 10 min at 4 °C and the supernatant was divided into two portions

for intact prodrug and DON release analysis. Disappearance of intact prodrugs from these samples were performed on a Dionex ultra-high-performance LC system coupled with Q Exactive Focus orbitrap mass spectrometer (Thermo Fisher Scientific Inc., Waltham MA). The separation of analytes was achieved using the Agilent Eclipse Plus column (100 × 2.1 mm i.d.; maintained at 35 ºC) packed with a 1.8 µm C18 stationary phase. The mobile phase consisted of 0.1% formic acid in water and 0.1% formic acid in acetonitrile. Pumps were operated at a flow rate of 0.4 mL/min for 9 min using gradient elution. The mass spectrometer controlled by Xcalibur software 4.0.27.13 (Thermo Scientific) was operated with a heated electrospray ionization (HESI) ion source in positive ionization mode. Quantification of the prodrugs were performed in the full-scan mode (from m/z 50 to 1600) by comparing t = 0 samples with t = 60 min samples. The DON release analysis in the 1h samples were performed using methods previously described(*37, 80*).

The plasma to tumor cell partition assay was performed using a previously reported method(*80*). Briefly, P493B lymphoma cells (obtained from Dr. Chi Dang, Abramson Cancer Center, University of Pennsylvania, Philadelphia, PA) were grown in 150 cm^2 cell T-flasks and upon confluency, cell pellets were collected by centrifugation of cell suspension at 200 × *g* for 5 min. Cell count was determined and cells were resuspended in human plasma (Innovative Research, Novi, MI) to obtain a cell density of 10 million cells/mL of plasma. This cell-plasma suspension was preincubated for 5 min at 37°C and spiked with respective prodrugs (final concentration of 20 µM) and re-incubated at 37 °C for 1 h. Following incubation, the cell suspension was centrifuged at 10,000 × *g* for 10 min at 4 °C and supernatant plasma was collected and stored at −80 °C until DON bioanalysis. The cell pellet was washed once with ice-cold Dulbecco's phosphate-buffered saline, followed by centrifugation and stored at −80 °C for DON bioanalysis as mentioned above.

Synthesis and characterization of DRP-104's M1 metabolite

L-Pyroglutamic acid (**1**) was refluxed with allyl alcohol in the presence of *p*-toluenesulfonic acid to give the allyl ester (**2d**). The amide nitrogen then was masked using Fmoc-Cl to give Fmoc-protected allyl ester of L-pyroglutamic acid (**3d**). Compound **3d** was transformed to allyl (*S*)-2-amino-6-diazo-5-oxohexanoate (**5d**) by cleavage of the C-N amide bond triggered by alkylation using trimethylsilyl diazomethane, followed by deprotection of the resulting Fmoc-amine. Compound **5d** was then coupled with Fmoc-protected L-tryptophan to yield the conjugate **6d** which was subsequently treated with acetic anhydride in presence of DMAP to replace the Fmoc moiety with acetyl (compound **8**). In the final step, intermediate **8** was subjected to palladium catalyzed de-allylation of the ester in presence of scavenger (phenyl silane) to yield **M1** (**9**). After purification on silica, compound **9** was isolated as a light yellow-orange solid in 54 % yield. All intermediates were isolated, purified and characterized using ^{1}H and ^{13}C NMR spectroscopy. NMR spectra and high-resolution MS characterization data of **M1** metabolite (**15**) are shown below.

^{1}H NMR (600 MHz, DMSO-d_6): 1.76 (d, *J* = 2.6 Hz, 3H), 1.78 – 1.85 (m, 1H), 1.96 – 2.05 (m, 1H), 2.26 – 2.42 (m, 2H), 2.89 (dd, *J* = 14.5, 9.8 Hz, 1H), 3.11 (dd, *J* = 15.0, 4.5 Hz, 1H), 4.16 (td, *J* = 8.3, 4.9 Hz, 1H), 4.54 (td, *J* = 9.0, 4.3 Hz, 1H), 6.03 (bs, 1H), 6.97 (t, *J* = 7.4 Hz, 1H), 7.05 (t, *J* = 7.5 Hz, 1H), 7.14 (d, *J* = 2.4 Hz, 1H), 7.32 (d, *J* = 8.0 Hz, 1H), 7.61 (d, *J* = 8.0 Hz, 1H), 8.02 (dd, *J* = 8.4, 4.0 Hz, 1H), 8.16 – 8.23 (m, 1H), 10.79 (bs, 1H). **HR ESI MS**: calcd for $C_{19}H_{20}O_5N_5$ 398.14699; found 398.14667.

Glutaminase (GLS-1) enzymatic activity assay

Compounds were screened as inhibitors of human kidney glutaminase (GLS-1) following a previously reported method(*41*, *81*). Briefly, recombinant GLS-1 was preincubated with either

DON, DRP-104 or M1 at room temperature (in 45mM phosphate pH 8.2) for up to 24h. At the end of the incubation period, the GLS-1 activity was measured with the addition of [^{3}H] labeled glutamine. The reaction was carried out for 45 minutes and subsequently terminated upon the addition of 20mM imidazole (pH 7.0). 96 well spin columns packed with strong anion exchange resins were used to separate the unhydrolyzed glutamine and the reaction product, [^{3}H] glutamate. [^{3}H] glutamine was removed by washing the spin columns with imidazole buffer and [^{3}H] glutamate was eluted with 0.1 M HCl and analyzed for radioactivity.

P493B cell viability assay

Cell proliferation assays were performed as previously published (*80*) using CellTiter 96 AQueous One Solution Cell Proliferation reagents following the manufacturers' instruction (Promega). Briefly, P493B lymphoma cells were grown in 150 cm^2 cell T-flasks and upon confluency, cells were harvested and cell count were determined. Cells were plated in 96-well plates at a density of 20,000 cells/well in a final volume of 100 μL of growth media. Test compound stocks were made in DMSO and were added to cells in a 1:10 serial dilution with a final concentration of 0.2% DMSO. Cells were allowed to proliferate for 72 h in the presence of each test compound. Thereafter, 20 μL of CellTiter 96 AQueous (Promega #3580) was added per well and incubated for 2 h. Absorbance was measured at 490 nm.

Tumor target engagement studies

EL4 tumor bearing C57BL/6/CES1$^{-/-}$ mice were dosed with vehicle (5% Ethanol + 10% Tween 80 + 85% PBS), DRP-104 (2.6 mg/kg) or DON (0.3 mg/kg) subcutaneously to provide equi-tumor exposures. Mice were sacrificed 1h post-administration, tumors were collected, and divided for analyses of DON, FGAR and GLS-1 activity. FGAR was quantified using ion-exchange LC-MS method as previously described(*45*). Briefly, ~50 mg of tumor samples was

processed by the addition of 5µL extraction solvent (methanol containing 10 µM deuterated N-Acetyl Aspartic acid (NAA-d3) as internal standard) per mg of tissue and homogenized with Spex® 2150 stainless steel beads at 1500 rpm for 3 min on Spex® Geno/Grinder® (Spex SamplePrep LLC, Metuchen, NJ, USA). Post homogenization, samples were centrifuged at 16,000 × *g* for 5 min at 4°C, and supernatants were diluted 5-fold in water and analyzed using the ion-exchange LC-MS method reported earlier(*45*).

Inhibition of glutaminase activity in the tumor samples was measured using a previously reported method(*41, 81*) as described above. Briefly, tumor homogenates (in ice-cold potassium phosphate buffer, 45 mM, pH 8.2) were incubated with [^{3}H]-glutamine (0.09 µM, 2.73 µCi) for 90 min at room temperature in 50 µL volumes in a 96-well microplate. The assay was terminated with imidazole buffer (20 mM, pH 7). 96-well spin columns packed with 200–400 mesh anion exchange resin (Bio-Rad) separated the substrate and reaction product. Unreacted [^{3}H]-glutamine was removed by washing with imidazole buffer and [^{3}H]-glutamate was eluted with 0.1 N HCl and analyzed for radioactivity using Perkin Elmer's TopCount instrument in conjunction with 96-well LumaPlates. Total protein was measured using BioRad's Detergent Compatible Protein Assay kit.

DON quantification in the tumor samples (following DON or DRP-104 treatment) were performed using a method previously described(*37, 80*) (*also described in the "Pharmacokinetics in mice" section in the main manuscript*).

DRP-104's preferential tumor delivery of DON in MC38, 3LL and E0771 tumor models

To ensure that DRP-104's tumor-targeting profile was not specific to E4 tumors, single time point PK evaluation was also conducted in three other syngeneic tumor models. MC38 cells were donated by CORVUS pharmaceuticals. 3LL cell lines were obtained from the American Type Culture Collection (ATCC). The E0771 cell line was purchased from CH3 BioSystems.

All cell lines were mycoplasma free via ELISA-based assays performed every 6 months. Briefly, MC38 (colon carcinoma) and 3LL (Lewis lung carcinoma) were cultured in DMEM based media with 10% fetal bovine serum (FBS). EL4 and E0771 cells were grown in RPMI based media with 10% FBS. Right flank of mice was injected with either EL4 (3×10^5 cells), MC38 (5×10^5 cells), 3LL (5×10^5 cells), or E0771 (2×10^5 cells) for tumor inoculations. Tumors were grown for 7-15 days until they reached 200 – 300 mm^3. Mice were dosed with subcutaneous DRP-104 (2.6 mg/kg) and sacrificed at 1-hour post-dose (n = 3 per group). Blood was collected by cardiac puncture and processed to plasma. Jejunum and tumors were harvested and all samples were flash frozen and stored at -80 ºC until analysis. DON quantification in the plasma, jejunum and tumor samples were performed using a method previously described(*37, 80*).

Pharmacokinetic evaluation of JHU-083 in C57BL/6/CES1$^{-/-}$ mice with EL4 tumors

JHU-083 was dosed (1mg/kg DON equivalent s.c.) to C57BL/6/CES1$^{-/-}$ mice bearing EL4 flank tumors as we have previously described(*37, 80*). Briefly, following JHU-083 administration, blood was collected via cardiac puncture and tissues (tumor and jejunum) were harvested at predetermined time points (0, 0.25, 0.5, 1, 3 and 6 h) and analyzed for DON release using the LC-MS/MS method as previously described(*37, 80*). Exposures were calculated (using WinNonlin version 8.3) and normalized with respect to tumor exposures to compare tumor penetration index versus plasma and GI tissue.

GI histopathological scoring from efficacy studies

GI tissues were isolated from the mice following the completion of the anti-tumor and tolerability studies and fixed in 10% formalin prior to being transferred to 70% ethanol. Samples were then shipped to IDEXX Bioanalytics (Columbia, MO) to be embedded in

paraffin, sectioned, and stained for hematoxylin and eosin (H&E). Blinded histopathological review was performed, both by IDEXX and internally at JHMI, followed by quantification of histological changes using a scoring rubric adapted from Erben et. al(*76*), that included metrics of inflammation (0-3) and architectural change (0-3), as detailed in **Figure S10**. Final images were acquired on a Zeiss LSM 800 microscope (Zeiss, Germany) using the brightfield settings and a magnification of 20X.

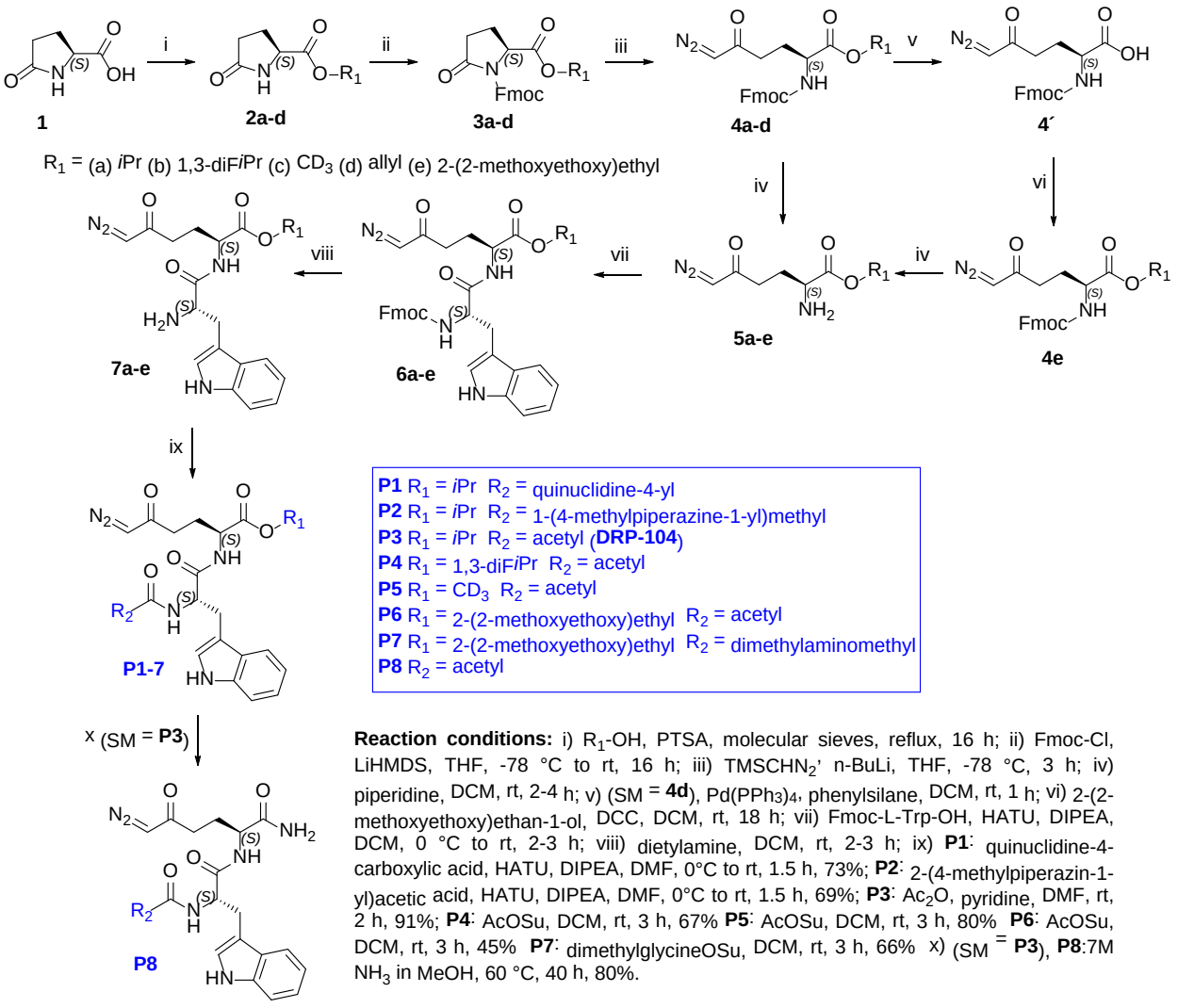

Reaction conditions: i) R_1-OH, PTSA, molecular sieves, reflux, 16 h; ii) Fmoc-Cl, LiHMDS, THF, -78 °C to rt, 16 h; iii) $TMSCHN_2$, n-BuLi, THF, -78 °C, 3 h; iv) piperidine, DCM, rt, 2-4 h; v) (SM = **4d**), $Pd(PPh_3)_4$, phenylsilane, DCM, rt, 1 h; vi) 2-(2-methoxyethoxy)ethan-1-ol, DCC, DCM, rt, 18 h; vii) Fmoc-L-Trp-OH, HATU, DIPEA, DCM, 0 °C to rt, 2-3 h; viii) dietylamine, DCM, rt, 2-3 h; ix) **P1**: quinuclidine-4-carboxylic acid, HATU, DIPEA, DMF, 0°C to rt, 1.5 h, 73%; **P2**: 2-(4-methylpiperazin-1-yl)acetic acid, HATU, DIPEA, DMF, 0°C to rt, 1.5 h, 69%; **P3**: Ac_2O, pyridine, DMF, rt, 2 h, 91%; **P4**: AcOSu, DCM, rt, 3 h, 67% **P5**: AcOSu, DCM, rt, 3 h, 80% **P6**: AcOSu, DCM, rt, 3 h, 45% **P7**: dimethylglycineOSu, DCM, rt, 3 h, 66% x) (SM = **P3**), **P8**:7M NH_3 in MeOH, 60 °C, 40 h, 80%.

Figure S1: Synthetic scheme and reaction conditions of prodrugs P1-P8

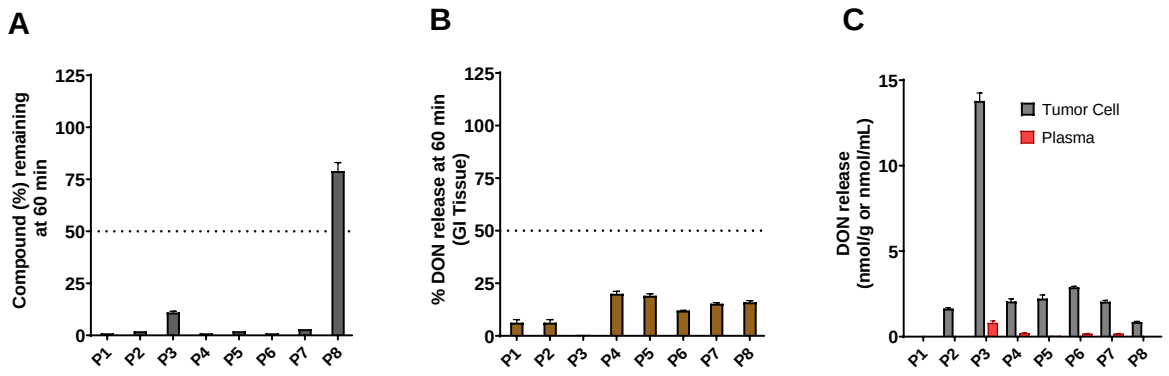

Figure S2: *In vitro* metabolic stability and DON release assessment of prodrugs P1-8. Metabolic stability of **P1-8** in (**A**) gastrointestinal tissue homogenates measuring intact prodrug remaining and (**B**) % DON release from the prodrugs in GI tissue homogenates after 60 min incubation at 37^0C. (**C**) Tumor cell partitioning of the prodrugs **P1-8** showing DON release in plasma and tumor cells.

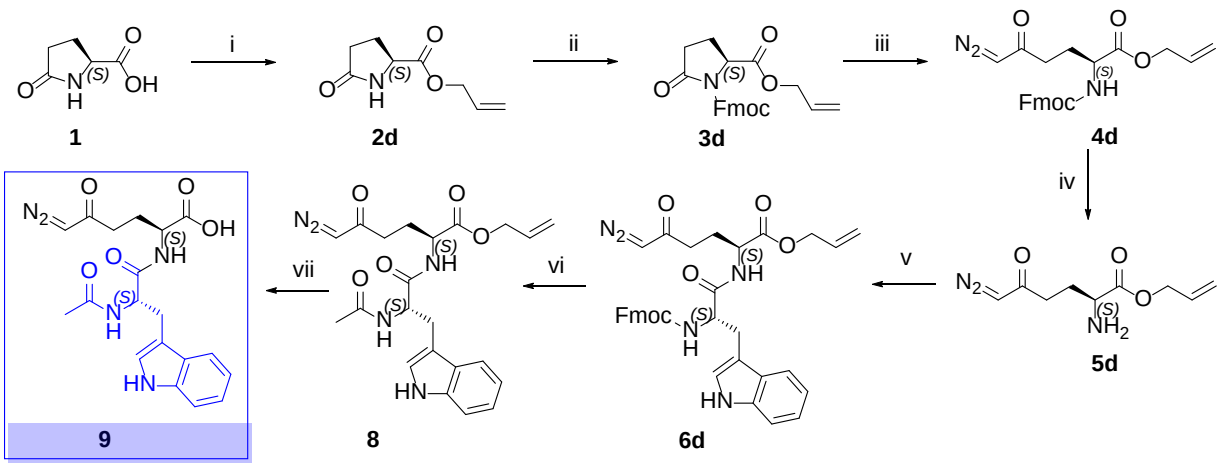

Reaction conditions: i) L-pyroglutamic acid, allyl alcohol, PTSA (cat.), molecular sieves, reflux, 18 h, 85%; ii) Fmoc-Cl, LiHMDS, THF, -78 °C to r.t., 19 h, 85%; iii) trimethylsilyl diazomethane, n-BuLi, THF, -116 to -78 °C, 3 h, 84%; iv) piperidine, DCM, r.t., 4 h, 71%; v) Fmoc-L-Trp-OH, HATU, DIPEA, DMF, 0 °C to r.t., 16 h, 76%; vi) Ac_2O, DMAP, DCM, 71 h, r.t., 79%; vii) $Pd(PPh_3)_4$, phenyl silane, DCM, r.t., 1 h, 54%.

Figure S3: Synthetic scheme/reaction conditions of DRP-104 M1 metabolite (compound 9).

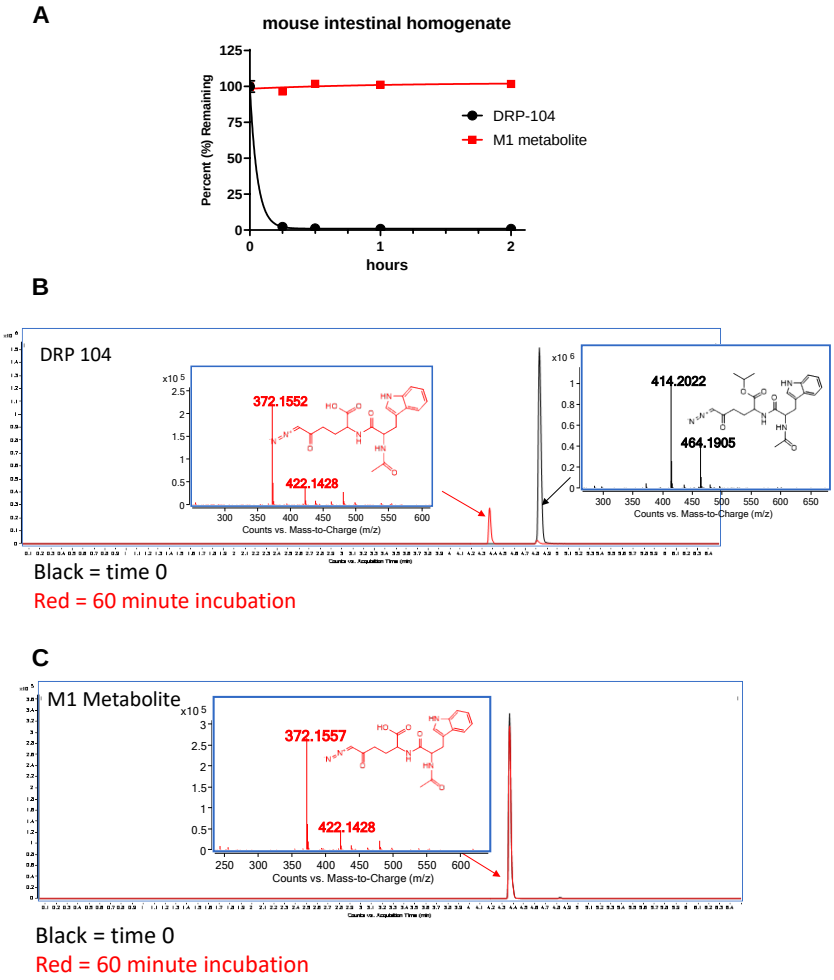

Figure S4. Stability comparison and metabolite identification of DRP-104 and its M1 metabolite in mouse intestinal homogenates and tumor homogenate. (A) DRP-104 was rapidly metabolized in mouse intestinal homogenate while its M1 metabolite showed complete stability. (**B**) Metabolite identification (MET-ID) studies showed metabolism of DRP-104 (m/z= 414.2022 ($-N_2+H^+$), m/z 464.1905 (+Na)) to M1 metabolite (m/z 372.1552). (**C**) MET-ID studies showed complete stability of M1 metabolite with no conversion to DON.

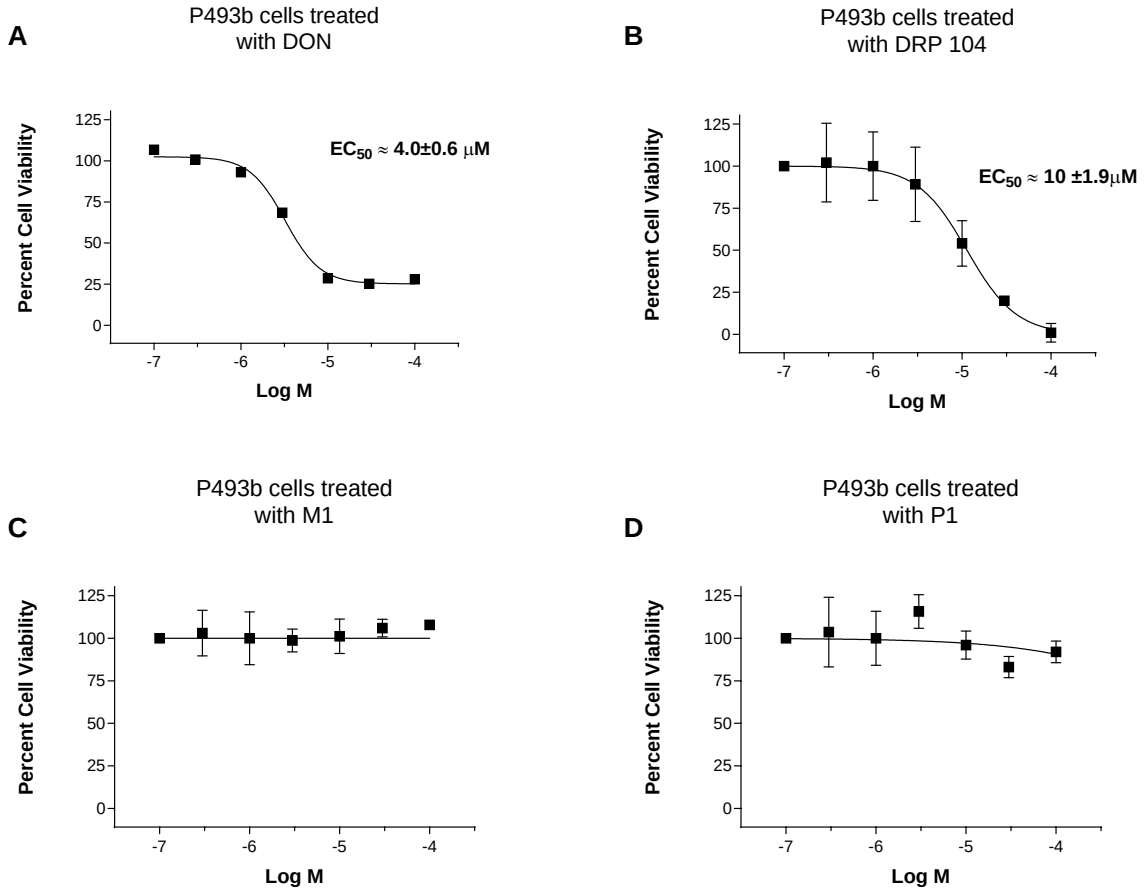

Figure S5: Dose-dependent antiproliferative effects of DON (A), DRP-104 (B), M1 metabolite (C), and prodrug P1 on P493b cells.

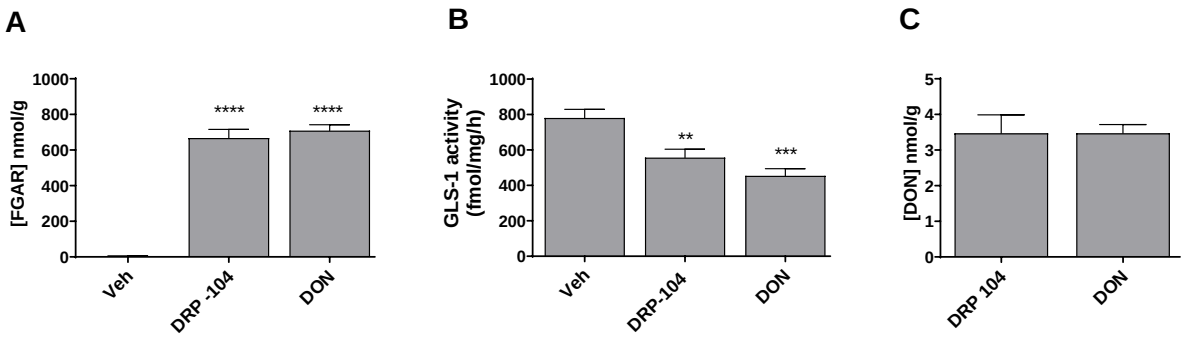

Figure S6: Assessment of DRP-104 tumor target engagement using FGAR (formylglycinamide ribonucleotide) and GLS activity *in vivo*. Quantification of tumor FGAR levels (**A**), glutaminase (GLS-1) activity (**B**), and DON concentration (**C**) following vehicle, DRP-104, or DON dosed subcutaneously in EL4 tumor bearing mice. (*****p < 0.0001, ***p <0.001 and **p < 0.01*, based on multiple t-tests; compared to vehicle group).

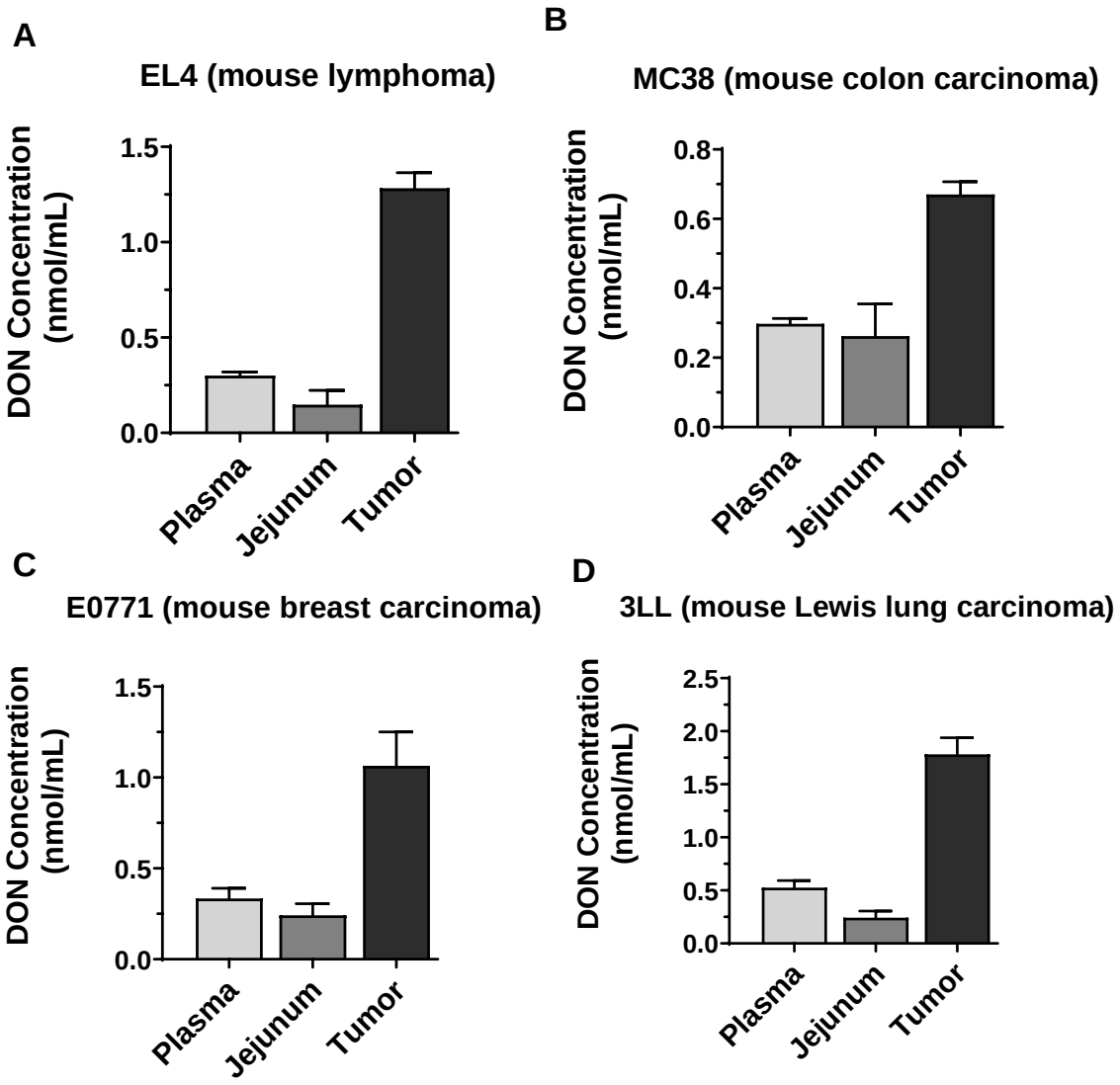

Figure S7: **DRP-104 shows preferential tumor delivery of DON.** DRP-104 (1 mg/kg s.c. DON equivalent) was administered to C57BL/6/CES1$^{-/-}$ mice bearing EL4 (**A**), MC38 (**B**), E0771 (**C**), or 3LL (**D**) flank tumors. Plasma, GI tissues and tumor were harvested and analyzed for DON 1h post administration. Like EL4 tumors, DON levels were 3-7-fold higher versus plasma and GI tissue confirming tumor specific delivery of DON via DRP-104.

A

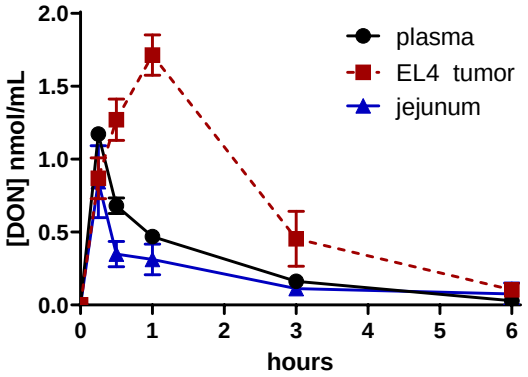

B

Pharmacokinetics of JHU-083 versus DRP-104			
Compound	**Matrix**	**AUC_{0-t} (nmol.h/mL or nmol.h/g)**	**Tumor Penetration Index ($AUC_{0-t\ (tumor/tissue)}$)**
DON (DRP-104)	Plasma	0.67±0.09	6.20
	Tumor	4.13±0.59	-
	GI	0.36±0.13	11.5
DON (JHU-083)	Plasma	1.58±0.06	2.6
	Tumor	4.13±0.55	-
	GI	1.12±0.28	3.69

Figure S8. Tumor Penetration Index (TPI) comparison of JHU-083 *versus* DRP-104 in mice with EL4 tumors. (**A**) Pharmacokinetic profile of DON from JHU-083 in plasma, tumor and GI tissue. (**B**) The TPI of DON afforded by JHU-083 were lower compared to DRP-104. TPI of DON from JHU-083 was 2.6 and 3.7 in plasma and GI tissues, respectively. TPI of DON from DRP-104 was 6.2- and 11.5 in plasma and GI tissues, respectively.

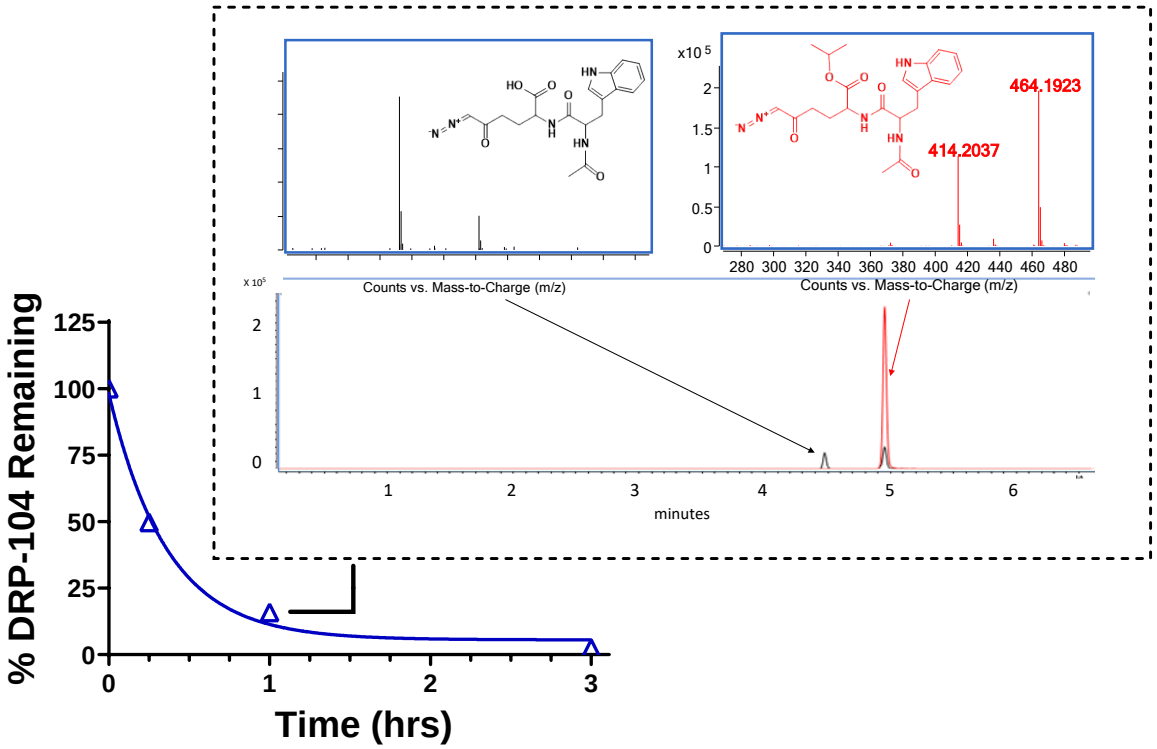

Figure S9. CES1-mediated metabolism of DRP-104. (A) DRP-104 is de-esterified to form M1 metabolite in presence of recombinant CES1 in a time dependent manner; **(B)** Red chromatogram represents incubation of DPR-104 in buffer without enzyme at 1h and black represents M1 metabolite in presence of recombinant CES1 enzyme.

A

Inflammation Score		
Severity	**Extent**	**Score 1**
Mild (<25%)	Mucosal	1
Moderate (25-50%)	Mucosal & Submucosal	2
Marked (>50%)	Transmural	3
Intestinal Architecture		
Epithelial Change	**Mucosal Architecture**	**Score 2**
Mild hyperplasia		1
Moderate hyperplasia	± occasional crypt dilation	2
Moderate hyperplasia	± frequent crypt dilation ± ulceration	3
GI Histopathology Score (Score 1 + Score 2):		0-6

B

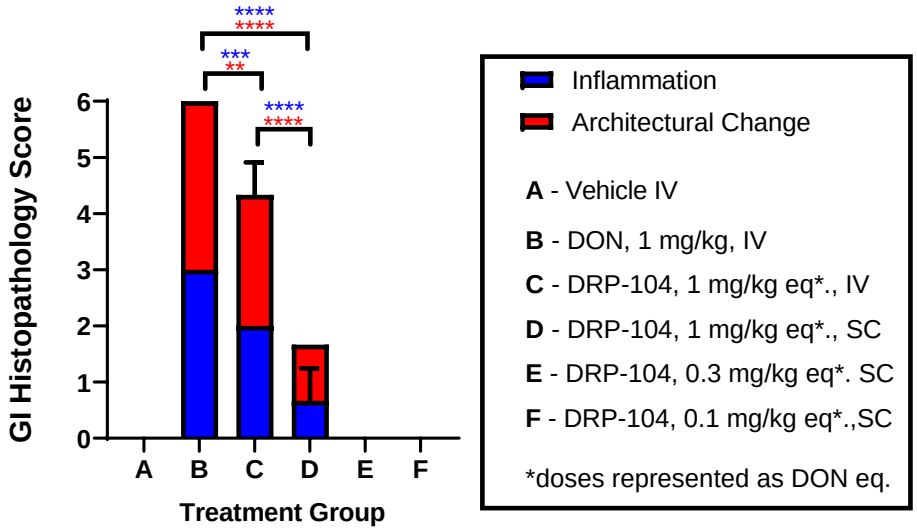

Figure S10. DRP-104 shows reduced GI toxicity relative to DON. (A) Quantitative gastrointestinal histopathological scoring was performed using a scoring rubric modified from Erben et al(*76*). (B) Similar to what has been reported previously, IV DON treatment resulted in severe GI toxicity including mucosal ulceration and diffuse transmural inflammation (**B**). In contrast, IV DRP-104 at an equimolar dose, had attenuated GI toxicity with significantly improved inflammation and architectural change scores. Reductions in GI toxicity were also observed when DRP-104 was administered SC rather than IV. *(**p<0.01, ***p<0.001, ****p<0.0001 2-way ANOVA*)

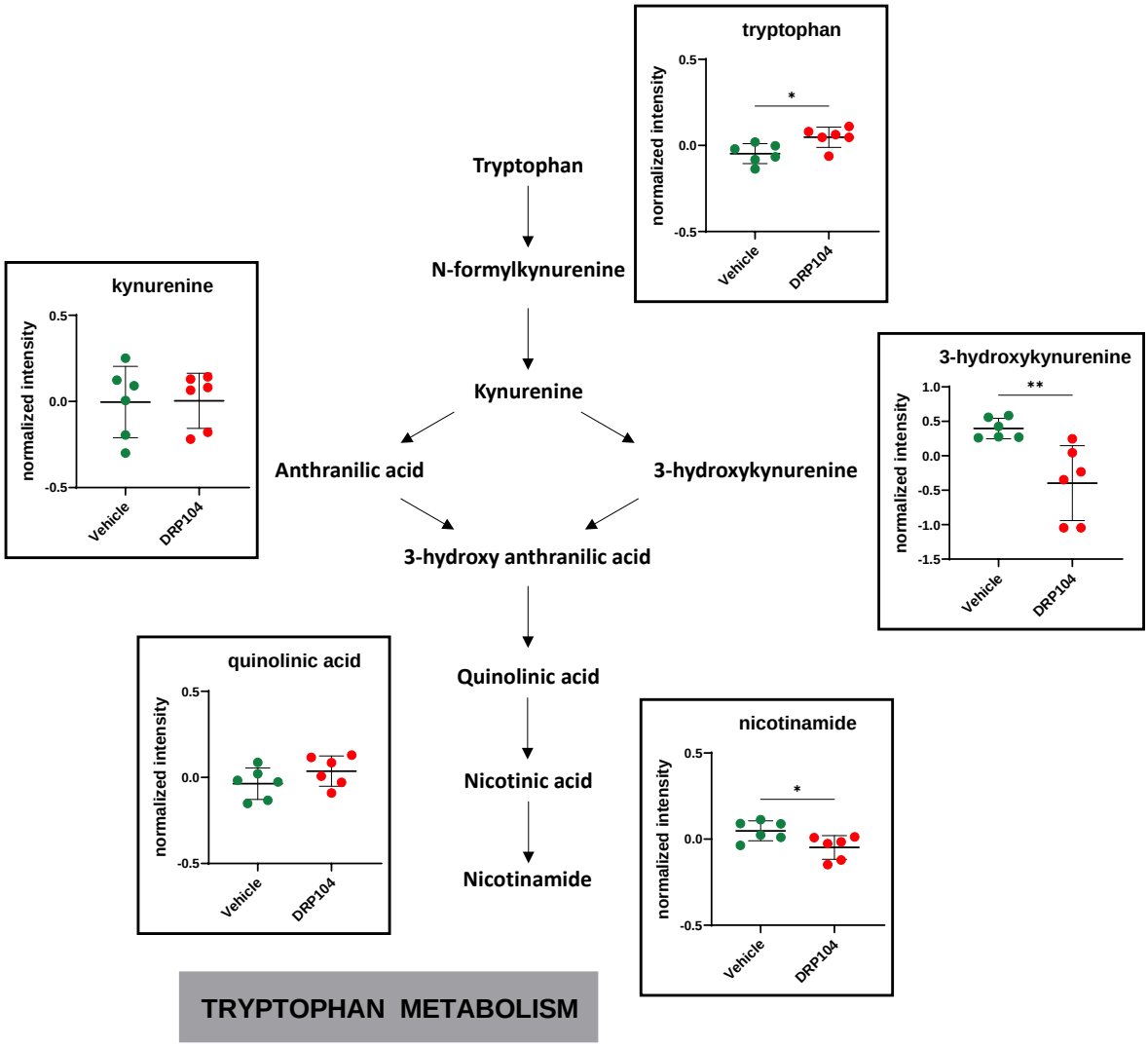

Figure S11: DRP-104 affects metabolites in the tryptophan/kynurenine pathway. Global metabolic profiling was performed following DRP-104 treatment (0.3 mg/kg DON eq dosed s.c. for 5 days) versus vehicle controls in EL4 bearing C57BL/6/CES1-/- mice. Several metabolites in the tryptophan/kynurenine pathway were significantly altered by DRP-104 treatment. *(*p<0.05, **p<0.01 by t-test)*

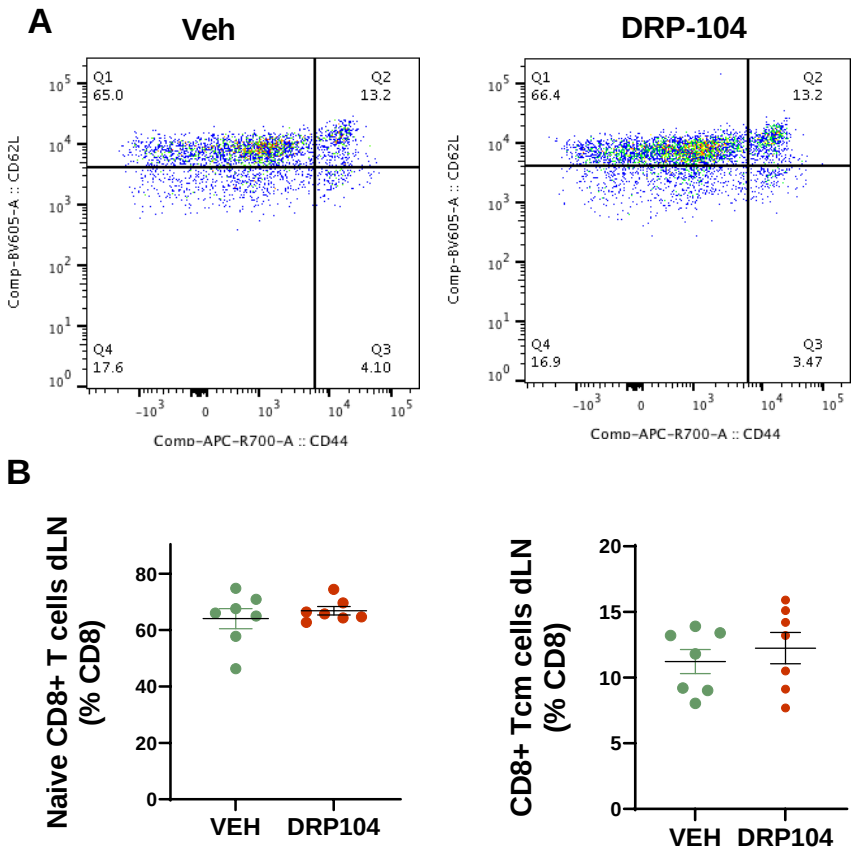

Figure S12. CD8+ T cells in draining lymph nodes are not significantly modulated in OVA-expressing MC38-bearing CES1$^{-/-}$ mice. OVA-expressing MC38-bearing CES1$^{-/-}$ mice treated with vehicle or DRP-104. Representative (**A**) flow cytometry plots and (**B**) data charts from Tetramer+ CD8+ lymphocytes from draining lymph nodes showing CD44 and CD62L.

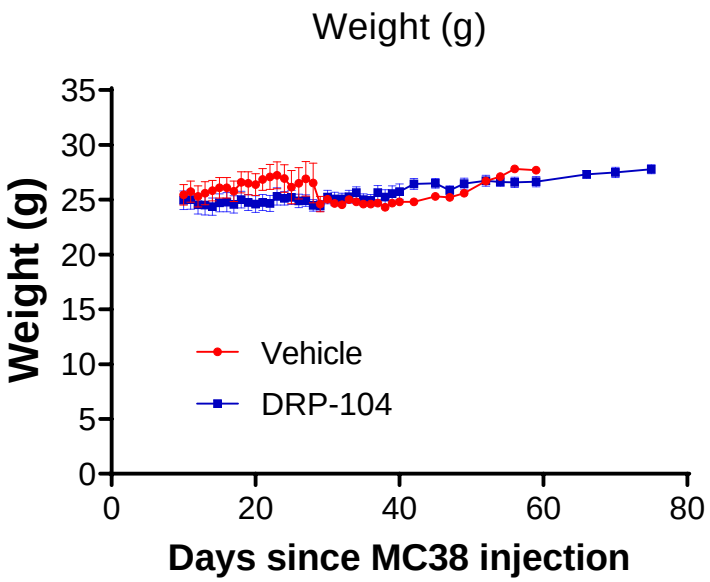

Figure S13. Administration of DRP-104 had no significant effect on body weight throughout the experiment. DRP-104 (0.3 mg/kg DON eq s.c. 5 days per week, 4 cycles) or vehicle were administered to MC38 tumor-bearing C57BL/6/CES1$^{-/-}$ mice from 10-36 days post-inoculation after which all drug therapy was discontinued. Data is shown for the entire experiment. (*Data until the first sacrifice is shown in* ***Fig.7B***)

Table S1: Inhibition of GLS-1 by DON, DRP-104 and M1 metabolite

	FW	**Average IC_{50} (µM)**
DON	171	10 ± 0.3
DRP-104	441	> 1000
M1 metabolite	399	> 1000

Table S2: Complete blood count (CBC) data from DON- and DRP-104-treated mice bearing EL4 tumors

Treatment	Animal	WBC (K/uL)	RBC (M/uL)	HGB (g/dL)	HCT (%)	MCV (*82*)	PLT (K/ul)	LYMPH (K/uL)
Vehicle *(iv)*	1	3.21	6.89	11.4	35.6	51.7	47*	1.56
	2	4.42	7.27	11.5	34.5	47.5	5*	3.82
	3	5.35	8.52	13.3	40.8	47.9	75	4.5
	Avg	**4.33**	**7.56**	**12.07**	**36.97**	**49.03**	**42.33**	**3.29**
DON *(1 mg/kg iv)*	1	1.22	5.45	8.7	24.2	44.4	254	0.69
	2	0.97*	4.99	7.7	21.8	43.7	613	0.57
	3	0.59*	3.23*	4.9*	13.5	41.8	503	0.48
	Avg	**0.93**	**4.56**	**7.10**	**19.83**	**43.30**	**456.67**	**0.58**
DRP-104 *(1 mg/kg eq. iv)*	1	6.93	5.18	8.1	23.4	45.2	562	1.96
	2	7.63	4.83	7.5	22	45.5	92	4.18
	3	2.9	4.34	6.8	20.4	47	884	1.69
	Avg	**5.82**	**4.78**	**7.47**	**21.93**	**45.90**	**512.67**	**2.61**
NORMAL RANGE		***1.06 - 56.08***	***3.57-15.2***	***6.1-21.7***	***16.7-69.8***	***39-90.8***	***59-2633***	***0.12-23.46***

*Values outside normal range

Table S3: Top significantly affected polar metabolites following DRP-104 treatment in mice bearing EL4 tumors

#	Name	FC	log2(FC)	raw.pval	neg log10(pval)	Metabolon Superpathway	Metabolon Subpathway
1	thiamin monophosphate	2.1274	1.0891	0.00025845	3.5876	Cofactors and Vitamins	Thiamine Metabolism
2	dehydroascorbate	2.2099	1.144	0.0031915	2.496	Cofactors and Vitamins	Ascorbate and Aldarate Metabolism
3	phosphopantetheine	0.26985	-1.8898	0.0099675	2.0014	Cofactors and Vitamins	Pantothenate and CoA Metabolism
4	carotene diol	2.2717	1.1838	0.027517	1.5604	Cofactors and Vitamins	Vitamin A Metabolism
5	hippurate	2.0784	1.0555	0.0084446	2.0734	Xenobiotics	Benzoate Metabolism
6	quinate	6.5264	2.7063	0.010951	1.9605	Xenobiotics	Food Component/Plant
7	cinnamoylglycine	2.0801	1.0566	0.014026	1.8531	Xenobiotics	Food Component/Plant
8	catechol sulfate	2.0923	1.0651	0.022124	1.6551	Xenobiotics	Benzoate Metabolism
9	pyrraline	0.49701	-1.0087	0.037152	1.43	Xenobiotics	Food Component/Plant
10	daidzein	0.46525	-1.1039	0.095273	1.021	Xenobiotics	Food Component/Plant
11	FGAR	17.258	4.1092	1.94E-06	5.7131	Nucleotide	Purine Metabolism, (Hypo)Xanthine/Inosine containing
12	(3'-5')-cytidylyluridine*	2.3519	1.2338	0.099711	1.0013	Nucleotide	Dinucleotide
13	adenine	0.17411	-2.5219	1.47E-05	4.834	Nucleotide	Purine Metabolism, Adenine containing
14	3'-AMP	3.1454	1.6532	0.0011047	2.9568	Nucleotide	Purine Metabolism, Adenine containing
15	2'-deoxyadenosine 5'-monophosphate	0.36406	-1.4578	0.0059188	2.2278	Nucleotide	Purine Metabolism, Adenine containing
16	2'-deoxyadenosine 3'-monophosphate	2.2097	1.1439	0.025054	1.6011	Nucleotide	Purine Metabolism, Adenine containing

17	ADP	2.1043	1.0733	0.06491	1.1877	Nucleotide	Purine Metabolism, Adenine containing
18	N2,N2-dimethylguanosine	0.42532	-1.2334	0.00019339	3.7136	Nucleotide	Purine Metabolism, Guanine containing
19	guanine	0.43383	-1.2048	0.0020562	2.6869	Nucleotide	Purine Metabolism, Guanine containing
20	guanosine 3'-monophosphate (3'-GMP)	2.5582	1.3552	0.0024416	2.6123	Nucleotide	Purine Metabolism, Guanine containing
21	2'-deoxyguanosine 3'-monophosphate	3.7745	1.9163	0.026211	1.5815	Nucleotide	Purine Metabolism, Guanine containing
22	5-methylcytidine	0.46723	-1.0978	0.00061986	3.2077	Nucleotide	Pyrimidine Metabolism, Cytidine containing
23	3'-CMP	2.3245	1.2169	0.0011607	2.9353	Nucleotide	Pyrimidine Metabolism, Cytidine containing
24	cytidine 2'-monophosphate (2'-CMP)	3.119	1.6411	0.002988	2.5246	Nucleotide	Pyrimidine Metabolism, Cytidine containing
25	cytidine 2',3'-cyclic monophosphate	4.1232	2.0438	0.0062983	2.2008	Nucleotide	Pyrimidine Metabolism, Cytidine containing
26	uridine 3'-monophosphate (3'-UMP)	3.3344	1.7374	0.0048689	2.3126	Nucleotide	Pyrimidine Metabolism, Uracil containing
27	uridine 2'-monophosphate (2'-UMP)*	2.4271	1.2792	0.0056489	2.248	Nucleotide	Pyrimidine Metabolism, Uracil containing
28	sucrose	3.255	1.7026	0.01911	1.7187	Carbohydrate	Disaccharides and Oligosaccharides
29	mannose	2.1235	1.0864	0.00041081	3.3864	Carbohydrate	Fructose, Mannose and Galactose Metabolism
30	galactonate	2.0887	1.0626	0.0008165	3.088	Carbohydrate	Fructose, Mannose and Galactose Metabolism
31	fructose	3.3603	1.7486	0.0043571	2.3608	Carbohydrate	Fructose, Mannose and Galactose Metabolism

32	glucose	4.2132	2.0749	0.0031968	2.4953	Carbohydrate	Glycolysis, Gluconeogenesis, and Pyruvate Metabolism
33	UDP-galactose	0.39817	-1.3286	0.012897	1.8895	Carbohydrate	Nucleotide Sugar
34	UDP-glucose	0.34993	-1.5149	0.014495	1.8388	Carbohydrate	Nucleotide Sugar
35	ribose	3.2264	1.6899	0.011928	1.9234	Carbohydrate	Pentose Metabolism
36	arabonate/xylonate	2.6375	1.3992	0.013149	1.8811	Carbohydrate	Pentose Metabolism
37	6-phosphogluconate	2.0405	1.0289	0.014256	1.846	Carbohydrate	Pentose Phosphate Pathway
38	ribulose/xylulose 5-phosphate	2.9922	1.5812	0.062116	1.2068	Carbohydrate	Pentose Phosphate Pathway
39	mesaconate (methylfumarate)	5.8113	2.5389	4.24E-05	4.3722	Energy	TCA Cycle
40	succinate	0.36295	-1.4621	0.052518	1.2797	Energy	TCA Cycle
41	succinylcarnitine (C4)	2.4981	1.3209	0.093724	1.0282	Energy	TCA Cycle
42	N-acetylaspartate (NAA)	3.2896	1.7179	4.23E-05	4.3738	Amino Acid	Alanine and Aspartate Metabolism
43	N,N-dimethylalanine	2.2461	1.1674	0.023005	1.6382	Amino Acid	Alanine and Aspartate Metabolism
44	creatinine	2.2503	1.1701	0.010825	1.9656	Amino Acid	Creatine Metabolism
45	N-acetylglutamate	2.3587	1.238	0.0011986	2.9213	Amino Acid	Glutamate Metabolism
46	glutamate, gamma-methyl ester	0.13195	-2.922	3.19E-07	6.4964	Amino Acid	Glutamate Metabolism
47	4-hydroxyglutamate	0.45319	-1.1418	0.01258	1.9003	Amino Acid	Glutamate Metabolism
48	cysteine-glutathione disulfide	4.1676	2.0592	0.00042693	3.3696	Amino Acid	Glutathione Metabolism
49	CoA-glutathione*	0.40991	-1.2866	0.0049451	2.3058	Amino Acid	Glutathione Metabolism
50	glutathione, reduced (GSH)	0.44864	-1.1564	0.086576	1.0626	Amino Acid	Glutathione Metabolism
51	S-lactoylglutathione	0.4664	-1.1004	0.099293	1.0031	Amino Acid	Glutathione Metabolism

52	betaine aldehyde	0.37158	-1.4283	0.055419	1.2563	Amino Acid	Glycine, Serine and Threonine Metabolism
53	1-methylguanidine	6.0586	2.599	0.0017371	2.7602	Amino Acid	Guanidino and Acetamido Metabolism
54	1-methylhistamine	2.5735	1.3637	0.00021751	3.6625	Amino Acid	Histidine Metabolism
55	1-methylhistidine	0.44355	-1.1728	0.0015546	2.8084	Amino Acid	Histidine Metabolism
56	imidazole lactate	0.45656	-1.1311	0.0033201	2.4789	Amino Acid	Histidine Metabolism
57	carnosine	4.8032	2.264	0.02965	1.528	Amino Acid	Histidine Metabolism
58	anserine	3.6378	1.8631	0.039976	1.3982	Amino Acid	Histidine Metabolism
59	methylsuccinate	5.9948	2.5837	6.99E-05	4.1553	Amino Acid	Leucine, Isoleucine and Valine Metabolism
60	2,3-dihydroxy-2-methylbutyrate	0.43761	-1.1923	0.010174	1.9925	Amino Acid	Leucine, Isoleucine and Valine Metabolism
61	4-methyl-2-oxopentanoate	2.7305	1.4492	0.019369	1.7129	Amino Acid	Leucine, Isoleucine and Valine Metabolism
62	5-(galactosylhydroxy)-L-lysine	2.5621	1.3573	3.07E-05	4.5135	Amino Acid	Lysine Metabolism
63	fructosyllysine	2.0861	1.0608	0.010589	1.9751	Amino Acid	Lysine Metabolism
64	homocysteine	0.17836	-2.4871	0.0032888	2.483	Amino Acid	Methionine, Cysteine, SAM and Taurine Metabolism
65	S-adenosylhomocysteine (SAH)	0.44096	-1.1813	0.004322	2.3643	Amino Acid	Methionine, Cysteine, SAM and Taurine Metabolism
66	2-hydroxy-4-(methylthio)butanoic acid	0.39521	-1.3393	0.0051349	2.2895	Amino Acid	Methionine, Cysteine, SAM and Taurine Metabolism
67	cystine	4.7395	2.2447	0.005961	2.2247	Amino Acid	Methionine, Cysteine, SAM and Taurine Metabolism
68	methionine sulfone	0.3029	-1.7231	0.016806	1.7745	Amino Acid	Methionine, Cysteine, SAM and Taurine Metabolism

69	hypotaurine	0.21449	-2.221	0.023144	1.6356	Amino Acid	Methionine, Cysteine, SAM and Taurine Metabolism
70	phenyllactate (*83*)	0.41418	-1.2717	0.010396	1.9831	Amino Acid	Phenylalanine Metabolism
71	N1,N12-diacetylspermine	0.49307	-1.0201	0.064378	1.1913	Amino Acid	Polyamine Metabolism
72	C-glycosyltryptophan	2.267	1.1808	0.00010068	3.997	Amino Acid	Tryptophan Metabolism
73	3-hydroxykynurenine	0.26055	-1.9403	0.0063243	2.199	Amino Acid	Tryptophan Metabolism
74	N-formylanthranilic acid	2.3088	1.2072	0.0168	1.7747	Amino Acid	Tryptophan Metabolism
75	indolelactate	0.37954	-1.3977	0.017011	1.7693	Amino Acid	Tryptophan Metabolism
76	indolepropionate	2.1608	1.1115	0.034388	1.4636	Amino Acid	Tryptophan Metabolism
77	phenol sulfate	2.8093	1.4902	0.012306	1.9099	Amino Acid	Tyrosine Metabolism
78	4-hydroxyphenylpyruvate	2.5858	1.3706	1.06E-05	4.9765	Amino Acid	Tyrosine Metabolism
79	prolylhydroxyproline	2.7349	1.4515	0.00015415	3.8121	Amino Acid	Urea cycle; Arginine and Proline Metabolism
80	2-oxoarginine*	2.2336	1.1594	0.0027397	2.5623	Amino Acid	Urea cycle; Arginine and Proline Metabolism
81	argininosuccinate	0.49219	-1.0227	0.0039391	2.4046	Amino Acid	Urea cycle; Arginine and Proline Metabolism
82	N,N,N-trimethyl-alanylproline betaine (TMAP)	2.8773	1.5247	0.024818	1.6052	Amino Acid	Urea cycle; Arginine and Proline Metabolism
83	leucylhydroxyproline*	2.6076	1.3827	0.00011729	3.9307	Peptide	Dipeptide Derivative
84	isoleucylhydroxyproline*	2.2685	1.1817	0.00016351	3.7865	Peptide	Dipeptide Derivative
85	tyrosylglycine	2.9042	1.5382	0.017576	1.7551	Peptide	Dipeptide
86	phenylalanylglycine	2.34	1.2265	0.023534	1.6283	Peptide	Dipeptide
87	alanylleucine	2.1317	1.092	0.025717	1.5898	Peptide	Dipeptide
88	valylglycine	2.6664	1.4149	0.095755	1.0188	Peptide	Dipeptide

FINAL REPORT OF LABORATORY EXAMINATION

4011 Discovery Drive, Columbia, MO 65201
1-800-669-0825 1-573-499-5700
idexxbioanalytics@idexx.com www.idexxbioanalytics.com

IDEXX BioAnalytics Case # 22608-2019

Received: 8/6/2019
Completed: 9/20/2009

Submitted By

Ying Wu
Johns Hopkins University
JJHD
855 N. Wolfe St
Room 265
Baltimore, MD 21205

Phone: 410-502-0497
Email: rrais2@jhmi.edu; ywu58@jhmi.edu

Specimen Description

Species: mouse
Breed/Strain: Ces1 KO/
Description: Tissues
Number of Specimens/Animals: 18
Study: LTP400 Tox Study

ID	Client ID	Species	Strain /Breed
1	Veh 1	mouse	Ces1 KO/
2	Veh 2	mouse	Ces1 KO/
3	Veh3	mouse	Ces1 KO/
4	DON 1mg/kg iv1	mouse	Ces1 KO/
5	DON 1mg/kg iv2	mouse	Ces1 KO/
6	DON 1mg/kg iv3	mouse	Ces1 KO/
7	LTP400 2.6mg/kg iv1	mouse	Ces1 KO/
8	LTP400 2.6mg/kg iv2	mouse	Ces1 KO/
9	LTP400 2.6mg/kg iv3	mouse	Ces1 KO/
10	LTP400 2.6mg/kg sc1	mouse	Ces1 KO/
11	LTP400 2.6mg/kg sc2	mouse	Ces1 KO/
12	LTP400 2.6mg/kg sc3	mouse	Ces1 KO/
13	LTP400 0.8mg/kg sc1	mouse	Ces1 KO/
14	LTP400 0.8mg/kg sc2	mouse	Ces1 KO/
15	LTP400 0.8mg/kg sc3	mouse	Ces1 KO/
16	LTP400 0.26mg/kg sc1	mouse	Ces1 KO/
17	LTP400 0.26mg/kg sc2	mouse	Ces1 KO/
18	LTP400 0.26mg/kg sc3	mouse	Ces1 KO/

Services/Tests Performed: Histopathology Services (1-18)

Histopathologic evaluation for: large intestine, small intestine

General Comments: Animals were dosed 5 days per week for two weeks. we are looking for toxicity in GI Track; Tissues - GI Track

Summary: Large and small intestinal segments were evaluated for tissue changes following administration of a compound at varying concentrations. Samples 4-6 have severe large intestinal tissue changes. Samples 7-12 have moderate to mild tissue changes. Please see the report for details.

HISTOPATHOLOGY

Animal: 1	
large intestine	no significant lesions
small intestine	no significant lesions

Animal: 2	
large intestine	no significant lesions
small intestine	no significant lesions

Animal: 3	
large intestine	no significant lesions
small intestine	no significant lesions

Animal: 4	
large intestine	Multifocally, there is severe mucosal epithelial ulceration, infiltration with abundant numbers of neutrophils and lymphocytes, and mats of abundant small bacilli immediately adjacent to the lesion. Multifocally, intact epithelium is moderately hyperplastic with a moderate amount of mucosal and transmural inflammatory infiltrates present (predominantly lymphocytes).
small intestine	no significant lesions

Animal: 5	
large intestine	Multifocally, there is severe mucosal epithelial ulceration, infiltration with abundant numbers of neutrophils and lymphocytes, and mats of abundant small bacilli immediately adjacent to the lesion. Multifocally, intact epithelium is moderately hyperplastic with a moderate amount of mucosal and transmural inflammatory infiltrates present (predominantly lymphocytes). Multifocally, there is moderate dilation of the crypts which contain inflammatory infiltrates and cellular debris.
small intestine	no significant lesions

Animal: 6	
large intestine	Multifocally, there is severe mucosal epithelial ulceration, infiltration with abundant numbers of neutrophils and lymphocytes, and mats of abundant small bacilli immediately adjacent to the lesion. Multifocally, intact epithelium is moderately hyperplastic with a moderate amount of mucosal and transmural inflammatory infiltrates present (predominantly lymphocytes). Multifocally, there is moderate dilation of the crypts which contain inflammatory infiltrates and cellular debris.
small intestine	no significant lesions

Animal: 7	
large intestine	Multifocally, there is moderate epithelial hyperplasia with a moderate amount of mucosal inflammatory infiltrates present (predominantly lymphocytes). Multifocally, there is dilation of the crypts which contain inflammatory infiltrates and cellular debris. The lamina propria has a severe amount of clear space within the interstitium (edema).
small intestine	no significant lesions

Animal: 8

large intestine	Multifocally, there is moderate epithelial hyperplasia with a moderate amount of mucosal inflammatory infiltrates present (predominantly lymphocytes). Multifocally, there is dilation of the crypts which contain inflammatory infiltrates and cellular debris. The lamina propria has a severe amount of clear space within the interstitium (edema).
small intestine	no significant lesions

Animal: 9	
large intestine	Multifocally, there are small areas of epithelial ulceration, mucosal infiltration with moderate numbers of neutrophils and lymphocytes. Multifocally, surrounding epithelium is moderately hyperplastic with occasional dilation of the crypts which contain inflammatory infiltrates and cellular debris. The lamina propria has a moderate amount of clear space within the interstitium (edema).
small intestine	no significant lesions

Animal: 10	
large intestine	Multifocal, mild epithelial hyperplasia and mild clear space within the interstitium of lamina propria (edema).
small intestine	no significant lesions

Animal: 11	
large intestine	Multifocal, mild epithelial hyperplasia and mild clear space within the interstitium of lamina propria (edema).
small intestine	no significant lesions

Animal: 12	
large intestine	Multifocal, mild epithelial hyperplasia and mild clear space within the interstitium of lamina propria (edema).
small intestine	no significant lesions

Animal: 13	
large intestine	no significant lesions
small intestine	no significant lesions

Animal: 14	
large intestine	no significant lesions
small intestine	no significant lesions

Animal: 15	
large intestine	no significant lesions
small intestine	no significant lesions

Animal: 16	
large intestine	no significant lesions
small intestine	no significant lesions

Animal: 17	
large intestine	no significant lesions
small intestine	no significant lesions

Animal: 18	
large intestine	no significant lesions
small intestine	no significant lesions

REFERENCES AND NOTES

1. D. Hanahan, R. A. Weinberg, Hallmarks of cancer: The next generation. *Cell* **144**, 646–674 (2011).

2. K. M. Lemberg, S. S. Gori, T. Tsukamoto, R. Rais, B. S. Slusher, Clinical development of metabolic inhibitors for oncology. *J. Clin. Invest.* **132**, e148550 (2022).

3. C. Hirayama, K. Suyama, Y. Horie, K. Tanimoto, S. Kato, Plasma amino acid patterns in hepatocellular carcinoma. *Biochem. Med. Metab. Biol.* **38**, 127–133 (1987).

4. R. J. DeBerardinis, A. Mancuso, E. Daikhin, I. Nissim, M. Yudkoff, S. Wehrli, C. B. Thompson, Beyond aerobic glycolysis: Transformed cells can engage in glutamine metabolism that exceeds the requirement for protein and nucleotide synthesis. *Proc. Natl. Acad. Sci. U.S.A.* **104**, 19345–19350 (2007).

5. J. S. Flier, M. M. Mueckler, P. Usher, H. F. Lodish, Elevated levels of glucose transport and transporter messenger RNA are induced by *ras* or *src* oncogenes. *Science* **235**, 1492–1495 (1987).

6. H. Ying, A. C. Kimmelman, C. A. Lyssiotis, S. Hua, G. C. Chu, E. Fletcher-Sananikone, J. W. Locasale, J. Son, H. Zhang, J. L. Coloff, H. Yan, W. Wang, S. Chen, A. Viale, H. Zheng, J. H. Paik, C. Lim, A. R. Guimaraes, E. S. Martin, J. Chang, A. F. Hezel, S. R. Perry, J. Hu, B. Gan, Y. Xiao, J. M. Asara, R. Weissleder, Y. A. Wang, L. Chin, L. C. Cantley, R. A. DePinho, Oncogenic Kras maintains pancreatic tumors through regulation of anabolic glucose metabolism. *Cell* **149**, 656–670 (2012).

7. D. Meynial-Denis, *Glutamine: Biochemistry, Physiology, and Clinical Applications* (CRC Press, 2017).

8. Y.-K. Choi, K.-G. Park, Targeting glutamine metabolism for cancer treatment. *Biomol. Ther.* **26**, 19–28 (2018).

9. D. R. Wise, C. B. Thompson, Glutamine addiction: A new therapeutic target in cancer. *Trends Biochem. Sci.* **35**, 427–433 (2010).

10. K. Thangavelu, C. Q. Pan, T. Karlberg, G. Balaji, M. Uttamchandani, V. Suresh, H. Schuler, B. C. Low, J. Sivaraman, Structural basis for the allosteric inhibitory mechanism of human kidney-type glutaminase (KGA) and its regulation by Raf-Mek-Erk signaling in cancer cell metabolism. *Proc. Natl. Acad. Sci. U.S.A.* **109**, 7705–7710 (2012).

11. R. J. Rosenbluth, D. A. Cooney, H. N. Jayaram, H. A. Milman, E. R. Homan, DON, CONV and DONV-II. Inhibition of L-asparagine synthetase in vivo. *Biochem. Pharmacol.* **25**, 1851–1858 (1976).

12. R. K. Barclay, M. A. Phillipps, Effects of 6-diazo-5-oxo-L-norleucine and other tumor inhibitors on the biosynthesis of nicotinamide adenine dinucleotide in mice. *Cancer Res.* **26**, 282–286 (1966).

13. G. S. Ahluwalia, J. L. Grem, Z. Hao, D. A. Cooney, Metabolism and action of amino acid analog anti-cancer agents. *Pharmacol. Ther.* **46**, 243–271 (1990).

14. B. Levenberg, I. Melnick, J. M. Buchanan, Biosynthesis of the purines. XV. The effect of aza-L-serine and 6-diazo-5-oxo-L-norleucine on inosinic acid biosynthesis de novo. *J. Biol. Chem.* **225**, 163–176 (1957).

15. M. L. Eidinoff, J. E. Knoll, B. Marano, L. Cheong, Pyrimidine studies: I. Effect of DON (6-diazo-5-oxo-L-norleucine) on incorporation of precursors into nucleic acid pyrimidines. *Cancer Res.* **18**, 105–109 (1958).

16. L. M. Pinkus, [45] Glutamine binding sites, in *Methods in Enzymology* (Elsevier, 1977), vol. 46, pp. 414–427.

17. H. W. Dion, S. A. Fusari, Z. L. Jakubowski, J. G. Zora, Q. R. Bartz, 6-Diazo-5-oxo-L-norleucine, a new tumor-inhibitory substance. II. Isolation and characterization. *J. Am. Chem. Soc.* **78**, 3075–3077 (1956).

18. R. D. Leone, L. Zhao, J. M. Englert, I. M. Sun, M. H. Oh, I. H. Sun, M. L. Arwood, I. A. Bettencourt, C. H. Patel, J. Wen, A. Tam, R. L. Blosser, E. Prchalova, J. Alt, R. Rais, B. S. Slusher, J. D. Powell, Glutamine blockade induces divergent metabolic programs to overcome tumor immune evasion. *Science* **366**, 1013–1021 (2019).

19. G. B. Magill, W. P. Myers, H. C. Reilly, R. C. Putnam, J. W. Magill, M. P. Sykes, G. C. Escher, D. A. Karnofsky, J. H. Burchenal, Pharmacological and initial therapeutic observations on 6-diazo-5-oxo-L-norleucine (DON) in human neoplastic disease. *Cancer* **10**, 1138–1150 (1957).

20. M. P. Sullivan, J. A. Nelson, S. Feldman, B. Van Nguyen, Pharmacokinetic and phase I study of intravenous DON (6-diazo-5-oxo-L-norleucine) in children. *Cancer Chemother. Pharmacol.* **21**, 78–84 (1988).

21. R. H. Earhart, D. J. Amato, A. Y. Chang, E. C. Borden, M. Shiraki, M. E. Dowd, R. L. Comis, T. E. Davis, T. J. Smith, Phase II trial of 6-diazo-5-oxo-L-norleucine versus aclacinomycin-A in advanced sarcomas and mesotheliomas. *Invest. New Drugs* **8**, 113–119 (1990).

22. A. Rahman, F. P. Smith, P. T. Luc, P. V. Woolley, Phase I study and clinical pharmacology of 6-diazo-5-oxo-L-norleucine (DON). *Invest. New Drugs* **3**, 369–374 (1985).

23. R. T. Eagan, S. Frytak, W. C. Nichols, E. T. Creagan, J. N. Ingle, Phase II study on DON in patients with previously treated advanced lung cancer. *Cancer Treat. Rep.* **66**, 1665–1666 (1982).

24. R. H. Earhart, J. M. Koeller, H. L. Davis, Phase I trial of 6-diazo-5-oxo-L-norleucine (DON) administered by 5-day courses. *Cancer Treat. Rep.* **66**, 1215–1217 (1982).

25. J. S. Kovach, R. T. Eagan, G. Powis, J. Rubin, E. T. Creagan, C. G. Moertel, Phase I and pharmacokinetic studies of DON. *Cancer Treat. Rep.* **65**, 1031–1036 (1981).

26. G. Lynch, N. Kemeny, E. Casper, Phase II evaluation of DON (6-diazo-5-oxo-L-norleucine) in patients with advanced colorectal carcinoma. *Am. J. Clin. Oncol.* **5**, 541–543 (1982).

27. A. A. Ovejera, D. P. Houchens, R. Catane, M. A. Sheridan, F. M. Muggia, Efficacy of 6-diazo-5-oxo-L-norleucine and *N*-[*N*-γ-glutamyl-6-diazo-5-oxo-norleucinyl]-6-diazo-5-oxo-norleucine against experimental tumors in conventional and nude mice. *Cancer Res.* **39**, 3220–3224 (1979).

28. J. Rubin, S. Sorensen, A. J. Schutt, G. A. van Hazel, M. J. O'Connell, C. G. Moertel, A phase II study of 6-diazo-5-oxo-L-norleucine (DON, NSC-7365) in advanced large bowel carcinoma. *Am. J. Clin. Oncol.* **6**, 325–326 (1983).

29. L. M. Shelton, L. C. Huysentruyt, T. N. Seyfried, Glutamine targeting inhibits systemic metastasis in the VM-M3 murine tumor model. *Int. J. Cancer* **127**, 2478–2485 (2010).

30. G. S. Tarnowski, C. C. Stock, Effects of combinations of azaserine and of 6-diazo-5-oxo-L-norleucine with purine analogs and other antimetabolites on the growth of two mouse mammary carcinomas. *Cancer Res.* **17**, 1033–1039 (1957).

31. R. Catane, D. D. Von Hoff, D. L. Glaubiger, F. M. Muggia, Azaserine, DON, and azotomycin: Three diazo analogs of L-glutamine with clinical antitumor activity. *Cancer Treat. Rep.* **63**, 1033–1038 (1979).

32. M. Sullivan, E. Beatty Jr, C. Hyman, M. Murphy, M. Pierce, N. Severo, A comparison of the effectiveness of standard dose 6-mercaptopurine, combination 6-mercaptopurine and DON, and high-loading 6-mercaptopurine therapies in treatment of the acute leukemias of childhood: Results of a coperative study. *Cancer Chemother. Rep.* **18**, 83–95 (1962).

33. C. T. Hensley, A. T. Wasti, R. J. DeBerardinis, Glutamine and cancer: Cell biology, physiology, and clinical opportunities. *J. Clin. Invest.* **123**, 3678–3684 (2013).

34. Calithera, Calithera Biosciences announces decision to discontinue KEAPSAKE clinical trial (2021).

35. C. Wyatt, J. M. Baeten, Tenofovir alafenamide for HIV infection: Is less more? *Lancet* **385**, 2559–2560 (2015).

36. M. T. Nedelcovych, L. Tenora, B.-H. Kim, J. Kelschenbach, W. Chao, E. Hadas, A. Jancarik, E. Prchalova, S. C. Zimmermann, R. P. Dash, A. J. Gadiano, C. Garrett, G. Furtmuller, B. Oh, G. Brandacher, J. Alt, P. Majer, D. J. Volsky, R. Rais, B. S. Slusher, *N*-(Pivaloyloxy)alkoxy-carbonyl prodrugs of the glutamine antagonist 6-diazo-5-oxo-L-norleucine (DON) as a potential treatment for HIV associated nseurocognitive disorders. *J. Med. Chem.* **60**, 7186–7198 (2017).

37. R. Rais, A. Jančařík, L. Tenora, M. Nedelcovych, J. Alt, J. Englert, C. Rojas, A. Le, A. Elgogary, J. Tan, L. Monincová, K. Pate, R. Adams, D. Ferraris, J. Powell, P. Majer, B. S. Slusher, Discovery of 6-diazo-5-oxo-L-norleucine (DON) prodrugs with enhanced CSF delivery in monkeys: A potential treatment for glioblastoma. *J. Med. Chem.* **59**, 8621–8633 (2016).

38. K. Y. Choi, M. Swierczewska, S. Lee, X. Chen, Protease-activated drug development. *Theranostics* **2**, 156–178 (2012).

39. N. Ueki, S. Lee, N. S. Sampson, M. J. Hayman, Selective cancer targeting with prodrugs activated by histone deacetylases and a tumour-associated protease. *Nat. Commun.* **4**, 2735 (2013).

40. P. L. Carl, P. K. Chakravarty, J. A. Katzenellenbogen, M. J. Weber, Protease-activated "prodrugs" for cancer chemotherapy. *Proc. Natl. Acad. Sci. U.S.A.* **77**, 2224–2228 (1980).

41. A. G. Thomas, C. Rojas, C. Tanega, M. Shen, A. Simeonov, M. B. Boxer, D. S. Auld, D. V. Ferraris, T. Tsukamoto, B. S. Slusher, Kinetic characterization of ebselen, chelerythrine and apomorphine as glutaminase inhibitors. *Biochem. Biophys. Res. Commun.* **438**, 243–248 (2013).

42. B. Li, M. Sedlacek, I. Manoharan, R. Boopathy, E. G. Duysen, P. Masson, O. Lockridge, Butyrylcholinesterase, paraoxonase, and albumin esterase, but not carboxylesterase, are present in human plasma. *Biochem. Pharmacol.* **70**, 1673–1684 (2005).

43. E. G. Duysen, F. Koentgen, G. R. Williams, C. M. Timperley, L. M. Schopfer, D. M. Cerasoli, O. Lockridge, Production of ES1 plasma carboxylesterase knockout mice for toxicity studies. *Chem. Res. Toxicol.* **24**, 1891–1898 (2011).

44. K. M. Lemberg, L. Zhao, Y. Wu, V. Veeravalli, J. Alt, J. M. H. Aguilar, R. P. Dash, J. Lam, L. Tenora, C. Rodriguez, M. T. Nedelcovych, C. Brayton, P. Majer, J. O. Blakeley, R. Rais, B. S. Slusher, The novel glutamine antagonist prodrug JHU395 has antitumor activity in malignant peripheral nerve sheath tumor. *Mol. Cancer Ther.* **19**, 397–408 (2020).

45. J. Alt, S. S. Gori, K. M. Lemberg, A. Pal, V. Veeravalli, Y. Wu, J. M. H. Aguilar, R. P. Dash, L. Tenora, P. Majer, Q. Sun, B. S. Slusher, R. Rais, Glutamine antagonist GA-607 causes a dramatic accumulation of FGAR which can be used to monitor target engagement. *Curr. Drug Metab.* **22**, 735–745 (2021).

46. A. Le, A. N. Lane, M. Hamaker, S. Bose, A. Gouw, J. Barbi, T. Tsukamoto, C. J. Rojas, B. S. Slusher, H. Zhang, L. J. Zimmerman, D. C. Liebler, R. J. Slebos, P. K. Lorkiewicz, R. M. Higashi, T.

W. Fan, C. V. Dang, Glucose-independent glutamine metabolism via TCA cycling for proliferation and survival in B cells. *Cell Metab.* **15**, 110–121 (2012).

47. R. J. DeBerardinis, T. Cheng, Q's next: The diverse functions of glutamine in metabolism, cell biology and cancer. *Oncogene* **29**, 313–324 (2010).

48. D. A. Tennant, R. V. Durán, E. Gottlieb, Targeting metabolic transformation for cancer therapy. *Nat. Rev. Cancer* **10**, 267–277 (2010).

49. K. M. Lemberg, J. J. Vornov, R. Rais, B. S. Slusher, We're not "DON" yet: Optimal dosing and prodrug delivery of 6-diazo-5-oxo-L-norleucine. *Mol. Cancer Ther.* **17**, 1824–1832 (2018).

50. F. Kratz, K. Abu Ajaj, A. Warnecke, Anticancer carrier-linked prodrugs in clinical trials. *Expert Opin. Investig. Drugs* **16**, 1037–1058 (2007).

51. C. Souza, D. S. Pellosi, A. C. Tedesco, Prodrugs for targeted cancer therapy. *Expert Rev. Anticancer Ther.* **19**, 483–502 (2019).

52. R. Mahato, W. Tai, K. Cheng, Prodrugs for improving tumor targetability and efficiency. *Adv. Drug Deliv. Rev.* **63**, 659–670 (2011).

53. H. He, L. Sun, J. Ye, E. Liu, S. Chen, Q. Liang, M. C. Shin, V. C. Yang, Enzyme-triggered, cell penetrating peptide-mediated delivery of anti-tumor agents. *J. Control. Release* **240**, 67–76 (2016).

54. Y. J. Zhong, L. H. Shao, Y. Li, Cathepsin B-cleavable doxorubicin prodrugs for targeted cancer therapy (Review). *Int. J. Oncol.* **42**, 373–383 (2013).

55. L.-H. Shao, S.-P. Liu, J.-X. Hou, Y.-H. Zhang, C.-W. Peng, Y.-J. Zhong, X. Liu, X.-L. Liu, Y.-P. Hong, R. A. Firestone, Y. Li, Cathepsin B cleavable novel prodrug Ac-Phe-Lys-PABC-ADM enhances efficacy at reduced toxicity in treating gastric cancer peritoneal carcinomatosis: An experimental study. *Cancer* **118**, 2986–2996 (2012).

56. J. Rautio, N. A. Meanwell, L. Di, M. J. Hageman, The expanding role of prodrugs in contemporary drug design and development. *Nat. Rev. Drug Discov.* **17**, 559–587 (2018).

57. A. Najjar, A. Najjar, R. Karaman, Newly developed prodrugs and prodrugs in development; an insight of the recent years. *Molecules* **25**, 884 (2020).

58. M. D. Kramer, P. Robinson, I. Vlodavsky, D. Barz, P. Friberger, Z. Fuks, V. Schirrmacher, Characterization of an extracellular matrix-degrading protease derived from a highly metastatic tumor cell line. *Eur. J. Cancer Clin. Oncol.* **21**, 307–316 (1985).

59. J. F. DiStefano, G. Beck, B. Lane, S. Zucker, Role of tumor cell membrane-bound serine proteases in tumor-induced target cytolysis. *Cancer Res.* **42**, 207–218 (1982).

60. J. A. Joyce, D. Hanahan, Multiple roles for cysteine cathepsins in cancer. *Cell Cycle* **3**, 1516–1519 (2004).

61. S. P. Sanghani, S. K. Quinney, T. B. Fredenburg, Z. J. Sun, W. I. Davis, D. J. Murry, O. W. Cummings, D. E. Seitz, W. F. Bosron, Carboxylesterases expressed in human colon tumor tissue and their role in CPT-11 hydrolysis. *Clin. Cancer Res.* **9**, 4983–4991 (2003).

62. P. D. Senter, K. S. Beam, B. Mixan, A. F. Wahl, Identification and activities of human carboxylesterases for the activation of CPT-11, a clinically approved anticancer drug. *Bioconjug. Chem.* **12**, 1074–1080 (2001).

63. B. Reigner, K. Blesch, E. Weidekamm, Clinical pharmacokinetics of capecitabine. *Clin. Pharmacokinet.* **40**, 85–104 (2001).

64. M. C. Bissery, P. Vrignaud, F. Lavelle, G. G. Chabot, Experimental antitumor activity and pharmacokinetics of the camptothecin analog irinotecan (CPT-11) in mice. *Anticancer Drugs* **7**, 437–460 (1996).

65. I. G. Kirwan, P. M. Loadman, D. J. Swaine, D. A. Anthoney, G. R. Pettit, J. W. Lippert, 3rd, S. D. Shnyder, P. A. Cooper, M. C. Bibby, Comparative preclinical pharmacokinetic and metabolic studies of the combretastatin prodrugs combretastatin A4 phosphate and A1 phosphate. *Clin. Cancer Res.* **10**, 1446–1453 (2004).

66. L. Shan, X. Zhuo, F. Zhang, Y. Dai, G. Zhu, B. C. Yung, W. Fan, K. Zhai, O. Jacobson, D. O. Kiesewetter, Y. Ma, G. Gao, X. Chen, A paclitaxel prodrug with bifunctional folate and albumin binding moieties for both passive and active targeted cancer therapy. *Theranostics* **8**, 2018–2030 (2018).

67. A. G. Thomas, C. M. O'Driscoll, J. Bressler, W. Kaufmann, C. J. Rojas, B. S. Slusher, Small molecule glutaminase inhibitors block glutamate release from stimulated microglia. *Biochem. Biophys. Res. Commun.* **443**, 32–36 (2014).

68. B. M. Liederer, R. T. Borchardt, Enzymes involved in the bioconversion of ester-based prodrugs. *J. Pharm. Sci.* **95**, 1177–1195 (2006).

69. K. M. Huttunen, H. Raunio, J. Rautio, Prodrugs—From serendipity to rational design. *Pharmacol. Rev.* **63**, 750–771 (2011).

70. R. H. Mathijssen, R. J. van Alphen, J. Verweij, W. J. Loos, K. Nooter, G. Stoter, A. Sparreboom, Clinical pharmacokinetics and metabolism of irinotecan (CPT-11). *Clin. Cancer Res.* **7**, 2182–2194 (2001).

71. M.-H. Oh, I.-H. Sun, L. Zhao, R. D. Leone, I.-M. Sun, W. Xu, S. L. Collins, A. J. Tam, R. L. Blosser, C. H. Patel, J. M. Englert, M. L. Arwood, J. Wen, Y. Chan-Li, L. Tenora, P. Majer, R. Rais, B. S. Slusher, M. R. Horton, J. D. Powell, Targeting glutamine metabolism enhances tumor-specific immunity by modulating suppressive myeloid cells. *J. Clin. Invest.* **130**, 3865–3884 (2020).

72. N. S. Sharma, V. K. Gupta, V. T. Garrido, R. Hadad, B. C. Durden, K. Kesh, B. Giri, A. Ferrantella, V. Dudeja, A. Saluja, S. Banerjee, Targeting tumor-intrinsic hexosamine biosynthesis sensitizes pancreatic cancer to anti-PD1 therapy. *J. Clin. Invest.* **130**, 451–465 (2020).

73. S. C. Zimmermann, T. Tichý, J. Vávra, R. P. Dash, C. E. Slusher, A. J. Gadiano, Y. Wu, A. Jančařík, L. Tenora, L. Monincová, E. Prchalová, G. J. Riggins, P. Majer, B. S. Slusher, R. Rais, N-substituted prodrugs of mebendazole provide improved aqueous solubility and oral bioavailability in mice and dogs. *J. Med. Chem.* **61**, 3918–3929 (2018).

74. L. Tenora, J. Alt, R. P. Dash, A. J. Gadiano, K. Novotna, V. Veeravalli, J. Lam, Q. R. Kirkpatrick, K. M. Lemberg, P. Majer, R. Rais, B. S. Slusher, Tumor-targeted delivery of 6-diazo-5-oxo-L-norleucine (DON) using substituted acetylated lysine prodrugs. *J. Med. Chem.* **62**, 3524–3538 (2019).

75. U. Erben, C. Loddenkemper, K. Doerfel, S. Spieckermann, D. Haller, M. M. Heimesaat, M. Zeitz, B. Siegmund, A. A. Kühl, A guide to histomorphological evaluation of intestinal inflammation in mouse models. *Int. J. Clin. Exp. Pathol.* **7**, 4557–4576 (2014).

76. A. M. Evans, B. Br, Q. Liu, M. W. Mitchell, R. Rj, H. Dai, S. Sj, C. D. DeHaven, M. Lad,, High resolution mass spectrometry improves data quantity and quality as compared to unit mass resolution mass spectrometry in high-throughput profiling metabolomics. *Metabolomics* **4**, 1–3 (2014).

77. C. D. Dehaven, A. M. Evans, H. Dai, K. A. Lawton, Organization of GC/MS and LC/MS metabolomics data into chemical libraries. *J. Cheminform.* **2**, 9 (2010).

78. J. Xia, D. S. Wishart, Using metaboanalyst 3.0 for comprehensive metabolomics data analysis. *Curr. Protoc. Bioinformatics* **55**, 14.10.11–14.10.91 (2016).

79. K. R. Hollinger, X. Zhu, E. S. Khoury, A. G. Thomas, K. Liaw, C. Tallon, Y. Wu, E. Prchalova, A. Kamiya, C. Rojas, S. Kannan, B. S. Slusher, Glutamine antagonist JHU-083 normalizes aberrant hippocampal glutaminase activity and improves cognition in APOE4 mice. *J. Alzheimers Dis.* **77**, 437–447 (2020).